

Satellite abundances around bright isolated galaxies

Wenting Wang^{1,2,3}, Simon D.M. White²

¹*Key Laboratory for Research in Galaxies and Cosmology of Chinese Academy of Sciences, Max-Planck-Institute Partner Group, Shanghai Astronomical Observatory, Nandan Road 80, Shanghai 200030, China*

²*Max Planck Institut für Astrophysik, Karl-Schwarzschild-Str. 1, 85741 Garching b. München, Germany*

³*Graduate School of the Chinese Academy of Sciences, 19A, Yuquan Road, Beijing, China, 100080*

Submitted to MNRAS

ABSTRACT

We study satellite galaxy abundances by counting photometric galaxies from the Eighth Data Release of the Sloan Digital Sky Survey (SDSS/DR8) around isolated bright primary galaxies from SDSS/DR7. We present results as a function of the luminosity, stellar mass and colour of the satellites, and of the stellar mass and colour of the primaries. For massive primaries ($\log M_*/M_\odot > 11.1$) the luminosity and stellar mass functions of satellites with $\log M_*/M_\odot > 8$ are similar in shape to those of field galaxies, but for lower mass primaries they are significantly steeper, even accounting for exclusion effects due to the isolation criteria. The steepening is particularly marked for the stellar mass function. Satellite abundance increases strongly with primary stellar mass, approximately in proportion to expected dark halo mass. For $\log M_*/M_\odot > 10.8$, red primaries have more satellites than blue ones of the same stellar mass. The effect exceeds a factor of two at $\log M_*/M_\odot \sim 11.2$. Satellite galaxies are systematically redder than field galaxies of the same stellar mass, except around primaries with $\log M_*/M_\odot < 10.8$ where their colours are similar or even bluer. Satellites are also systematically redder around more massive primaries. At fixed primary mass, they are redder around red primaries. We select similarly isolated galaxies from mock catalogues based on the galaxy formation simulations of Guo et al. and analyze them in parallel with the SDSS data. The simulation reproduces all the above trends qualitatively, except for the steepening of the satellite luminosity and stellar mass functions with decreasing primary mass. Model satellites, however, are systematically redder than in the SDSS, particularly at low mass and around low-mass primaries. Simulated haloes of a given mass have satellite abundances that are independent of central galaxy colour, but red centrals tend to have lower stellar masses, reflecting earlier quenching of star formation by feedback. This explains the correlation between satellite abundance and primary colour in the simulation. The correlation between satellite colour and primary colour arises because red centrals live in haloes which are more massive, older and more gas-rich, so that satellite quenching is more efficient.

Key words: galaxies:abundances-galaxies:evolution-galaxies:luminosity function, mass function-galaxies:statistics-cosmology:observations-cosmology:dark matter

1 INTRODUCTION

Clustering studies provide insights into the formation and evolution of galaxies that complement those coming from the joint distribution of intrinsic properties – mass, size, morphology, gas content, star-formation rate, nuclear activity, characteristic velocity and metallicity. In particular, clustering studies connect galaxies to their unseen dark matter haloes and indicate how these were assembled. According to the current standard Λ CDM paradigm, galaxies form as gas cools and condenses at the centres of a hierarchically aggregating population of dark matter haloes, as originally

outlined by White & Rees (1978). As smaller haloes fall into more massive ones, their central galaxies become satellites of these new hosts, occasionally merging at some later time into the new central galaxies in their cores. Thus, each halo contains a dominant galaxy at the bottom of its potential well, and a set of satellites which were the central galaxies of smaller progenitors. Observational studies of satellite populations provide a check on this picture, indicating how central galaxy properties relate to halo mass, and how these properties are modified when a halo falls into a bigger system.

The abundance of satellites, their spatial distribution and their intrinsic properties are thus intimately bound up with halo merger histories, which are themselves closely related to the underlying cosmology. For example, the evolution of merger rates is sensitive to the cosmic matter density, while the mass distribution of merging objects depends on the linear power spectrum of initial density fluctuations (Lacey & Cole 1993). Thus, satellite properties can, in principle, be used to constrain cosmological parameters. On the other hand, the physical processes driving galaxy evolution have strong effects on satellites. For example, their colours are affected by stripping of the gas reservoirs which supply star formation, and both gravitational and hydrodynamical processes can modify their structure, changing their morphology and partially or even totally disrupting them. Modern evolutionary models for the galaxy population attempt to include such processes and can be tested by comparison with the abundances, colours and spatial distributions of satellites.

The “missing satellite problem” is a particularly striking example of how satellite galaxy studies can constrain cosmology and galaxy evolution. The problem highlights an apparent mismatch between the large number of self-bound subhaloes found in Λ CDM simulations of the formation of haloes like those of the Milky Way and M 31, and the much smaller number of satellite galaxies observed around these two Local Group galaxies (Klypin et al. 1999; Moore et al. 1999; Kravtsov, Gnedin, & Klypin 2004). This discrepancy has traditionally been addressed by claiming that photoionisation and supernova feedback suppress cooling and star formation in low-mass haloes, so that only the most massive Milky Way subhaloes were able to make stars, the rest remaining dark (e.g. Kauffmann, White, & Guiderdoni 1993; Bullock, Kravtsov, & Weinberg 2000; Benson et al. 2002; Somerville 2002; Macciò et al. 2010; Guo et al. 2011). Recent analyses of the kinematics of Galactic satellites suggest, however, that their dark matter haloes are not dense enough to correspond to the most massive subhaloes in a Λ CDM universe (Boylan-Kolchin, Bullock, & Kaplinghat 2012; Ferrero et al. 2011). Such problems have led a number of authors to invoke warm dark matter (WDM) to eliminate subhaloes less massive than a few billion solar masses, and to reduce the central density of subhaloes above this cut-off (e.g. Moore et al. 2000; Spergel & Steinhardt 2000; Yoshida et al. 2000; Bode, Ostriker, & Turok 2001; Zavala et al. 2009; Lovell et al. 2012). Others claim that part of the problem may be incompleteness of the observed satellite population (e.g., Willman et al. 2004; Simon & Geha 2007; Koposov et al. 2008; Tollerud et al. 2008; Walsh, Willman, & Jerjen 2009).

Two kinds of methods are now commonly used to compare galaxy clustering in large redshift surveys to the predictions of high-resolution simulations of cosmic structure formation. The Halo Occupation Distribution (HOD; e.g., Jing, Mo, & Boerner 1998; Jing & Boerner 1998; Peacock & Smith 2000; Ma & Fry 2000; Seljak 2000; Berlind and Weinberg 2002; Cooray & Sheth 2002; Zheng et al. 2005) and the closely related Conditional Luminosity Function (CLF; Yang, Mo, & van den Bosch 2003) approaches determine the central and satellite galaxy populations of haloes as a function of mass by optimizing the fit to abundance and clustering observations, typically lumi-

osity and correlation functions. In a non-parametric variant, the observed abundance of central galaxies is matched directly to the simulated abundance of haloes to obtain a monotonic relation between galaxy luminosity and halo mass (Abundance Matching, AM; Tasitsiomi et al. 2004; Vale & Ostriker 2004; Conroy, Wechsler, & Kravtsov 2006; Moster et al. 2010; Guo et al. 2010). This relation can be used to populate both main and satellite subhaloes, if it is assumed to hold when satellites first fall into more massive systems. By construction, these methods fit observed luminosity functions perfectly. The same is true for observed correlation functions for HOD and CLF, whereas these serve as a test for AM. None of these schemes explains *why* haloes of given mass have central galaxies with specific properties.

In contrast, semi-analytic models use simplified representations of the relevant astrophysics to follow galaxy growth within the evolving dark halo population, and so attempt to predict the detailed properties of both central and satellite galaxies (SAM; e.g., White & Frenk 1991; Kauffmann, White, & Guiderdoni 1993; Cole et al. 1994; Kauffmann et al. 1999; Somerville & Primack 1999; Springel et al. 2001; Kang et al. 2005). Here, adjustable parameters correspond to the efficiencies of poorly understood processes like star formation or AGN feedback, so that the values derived from fitting to observation are interesting in their own right. In recent years, ever more detailed astrophysical models have been incorporated into ever larger and higher resolution simulations of dark matter evolution, leading to increasingly faithful representation of the observed galaxy population (e.g. Springel et al. 2005; Croton et al. 2006; Bower et al. 2006; De Lucia & Blaizot 2007; Guo et al. 2011).

Many studies of satellite galaxy populations have focused on the Local Group (LG) because of the greater depth and detail with which nearby galaxies can be studied (see Grebel (2000, 2001, 2007, 2011) and references therein). Recent work has been particularly concerned with comparing Λ CDM predictions to the abundance and internal structure of dwarf spheroidal galaxies and to the orbital and internal properties of the Magellanic Clouds (e.g. Koposov et al. 2009; Liu et al. 2011; Font et al. 2011; Tollerud et al. 2011; Sales et al. 2011; Boylan-Kolchin, Bullock, & Kaplinghat 2011). Such studies are limited by the fact that the LG contains only two large spirals, since considerable scatter is expected among the satellite populations of similar mass haloes (e.g. Boylan-Kolchin et al. 2010; Guo et al. 2011).

Beyond the LG, many observational studies of satellite populations have estimated their luminosity functions and their radial distribution around their primaries, but rather few have compared directly with theoretical expectations. Some studies have used redshift surveys to investigate the projected number density profiles of satellites (e.g. Vader & Sandage 1991; Sales & Lambas 2005; Chen et al. 2006) usually fitting power laws $\Sigma(r) \sim r^\alpha$, and obtaining slopes α between -0.5 and -1.2 . The availability of redshifts for all galaxies facilitates discrimination between satellites and background objects, but, for most objects, satellites are detectable only one or two magnitudes fainter than their primaries. An important application made possible by the redshifts is the measurement of mean dynamical masses for haloes as a function of central galaxy luminosity and colour

(Zaritsky et al. 1993, 1997; Prada et al. 2003; Conroy et al. 2005, 2007; More et al. 2011). The last of these papers finds that, at given luminosity, red central galaxies have more massive haloes than blue ones, but that this difference goes away if red and blue primaries are compared at the same stellar mass. We will return to this issue below.

The abundance of satellites at magnitudes much fainter than their primaries is most easily studied by combining a redshift survey with a photometric survey which catalogues galaxies several magnitudes below the spectroscopic limit. In the absence of redshifts, it is not possible, of course, to distinguish true satellites from background galaxies. Results can therefore be obtained only by stacking large samples of primaries so that a statistical subtraction of the background population is possible (Holmberg 1969; Phillipps & Shanks 1987; Lorrimer et al. 1994; Smith, Martínez, & Graham 2004; Tal et al. 2012). In particular, Lorrimer et al. (1994) counted the number of faint images on Schmidt survey plates around primaries of known redshift, using a “bootstrap” method to remove the background and fitting the projected surface density to a power law $\Sigma(r_p) \sim r_p^{-\alpha}$, finding $\alpha \sim 0.9$. They showed that satellites are more abundant and are concentrated to smaller radii around early-type primaries than around late-types.

Most recent work has taken advantage of the enormous increase in data provided by the Sloan Digital Sky Survey (SDSS; York et al. 2000). Weinmann et al. (2006) used the group catalogue of Yang et al. (2007), constructed from the SDSS spectroscopic data, to study in detail how the properties of satellite galaxies depend on the colour, luminosity, and morphology of the central galaxy and on their inferred dark halo mass. They compared their observational results with a mock redshift survey based on the SAM of Croton et al. (2006), finding significant discrepancies. In particular, the model overpredicted the number of faint satellites in massive haloes and produced too many red satellites. The fraction of blue central galaxies was also too high at high luminosities. Weinmann et al. (2006) argued that the satellite problems most likely reflect an improper treatment of tidal stripping or of the truncation of star formation, while the central problem may reflect an overly simple treatment of dust or of AGN feedback. In Weinmann et al. (2011) a mock catalog based on the more recent model of Guo et al. (2011) was compared with several nearby galaxy clusters as well as with the group catalogue of Yang et al. (2007). Discrepancies were weaker than for the earlier model, but the predicted fraction of red dwarf satellites remains higher than in the Virgo cluster or in the group catalogue of Yang et al. (2007), although agreeing with the fractions found in the Coma and Perseus clusters.

Studies of satellite galaxies based on both spectroscopic and photometric data from the SDSS have been published recently by Lares, Lambas, & Domínguez (2011), by Guo et al. (2011) and by Tal et al. (2012); Tal, Wake, & van Dokkum (2012). The first of these investigated how the luminosity function and number density profile of satellites depend on the colour and luminosity of their central galaxy, finding the abundance of satellites to depend strongly on primary luminosity, and the faint-end slope of their luminosity function to be consistent with that of the field. Using similar datasets, Guo et al. (2011) investigated the satellite luminosity function and its dependence on pri-

mary luminosity, colour and concentration. Their satellite luminosity function estimates are not well fit by Schechter functions, tending to be flat at bright luminosities but very steep at faint luminosities, apparently at odds with the conclusions of Lares, Lambas, & Domínguez (2011). For the primary magnitude range ($M_V = -21.25 \pm 0.5$) the mean luminosity function of Guo et al. (2011) is similar in shape to that of the MW and M31, but the abundance of satellites is about a factor two lower. Tal et al. (2012) studied satellites of SDSS Luminous Red Galaxies using, in particular, the deep Stripe 82 data finding a luminosity function with a shallow faint end slope and a very different shape from those of Guo et al. (2011). Tal, Wake, & van Dokkum (2012) constructed radial number density profiles for these same systems, concluding that they are well fitted by a NFW model (Navarro, Frenk, & White 1996, 1997) on large scales while at small radii there is an excess of satellites compared with the NFW profile, which can be well described by a Sersic model. Using data from the Galaxy and Mass Assembly Survey (GAMA; Driver et al. 2009, 2011), Prescott et al. (2011) also studied satellite number density profiles and red fractions as functions of projected separation and the masses of both satellite and primary, arguing that their results favour removal of gas reservoirs as the main mechanism quenching star formation in satellites. Finally, Nierenberg et al. (2012) use HST data from the Cosmological Evolution Survey (COSMOS) to study similar issues for smaller samples of galaxies, but out to $z \sim 0.8$.

In the present paper we return to many of these questions, using the full SDSS spectroscopic and photometric databases in conjunction with the galaxy population simulations of Guo et al. (2011, hereafter G11). The simulations allow us to compare expectations based on our current understanding of galaxy formation in a Λ CDM universe with the observed dependences of satellite luminosity, stellar mass and colour on primary galaxy properties. By using mock catalogues from the simulations, we are able to explore how satellite populations relate to the dark matter haloes in which they are embedded, to gain insight into the effect of physical processes like quenching and tidal stripping on their observable properties, and to explore how the observational criteria defining isolated primary galaxies impact the clustering of other galaxies around them (see Fall et al. (1976) for an old example of the potential strength of such effects).

We describe the datasets we use and the selection criteria which define our primary and satellite galaxy samples in section 2. In section 3 we introduce our background subtraction method. We present our SDSS results and compare them directly with the G11 simulation in sections 4 and 5. Further discussion and comparison with previous work is given in our concluding section. An appendix describes a variety of tests for systematics in the SDSS photometric data and in the techniques we use to correct satellite counts for contamination by foreground and background galaxies. Throughout this paper, we convert observational to intrinsic properties assuming a cosmology with $\Omega_m = 0.25$, $\Omega_\Lambda = 0.75$ and $h = 0.73$. We quote all masses in units of M_\odot rather than $h^{-1}M_\odot$.

2 DATA AND SAMPLE SELECTION

2.1 Primary Selection

We wish to study the satellite populations of bright isolated galaxies out to distances ~ 0.5 Mpc. We begin by considering all galaxies brighter than $r = 16.6$ (r -band extinction corrected Petrosian magnitude) in the spectroscopic galaxy catalogue of the New York University Value Added Galaxy Catalog (NYU-VAGC)¹ (Aihara et al. 2011). This catalogue was built by Blanton et al. (2005) on the basis of the seventh Data Release of the Sloan Digital Sky Survey (SDSS/DR7; Abazajian et al. 2009). This apparent magnitude limit provides us with a parent catalogue of 145070 objects. We select isolated galaxies from this sample by requiring that there should be no companion in the spectroscopic sample at $r_p < 0.5$ Mpc and $|\Delta z| < 1000$ km/s that is less than a magnitude fainter in r than the central object, and no companion at $r_p < 1$ Mpc and $|\Delta z| < 1000$ km/s that is brighter than it. These isolation criteria reduce our sample to 66285 objects.

The SDSS spectroscopic sample is incomplete, because observing efficiency constraints made it impossible to put a fibre on all candidates or to re-observe objects where an initial spectrum yielded an unreliable redshift. The completeness varies with position on the sky and has a mean of 91.5% for our parent sample. Thus $\sim 10\%$ of our “isolated” galaxies will not, in fact, be isolated according to our criteria, because their companion was missed by the spectroscopic survey. To eliminate such systems we apply an additional cut using the SDSS photometric data. The photometric redshift 2 catalogue (photoz2; Cunha et al. 2009) on the SDSS website provides redshift probability distributions for all galaxies in the SDSS footprint down to apparent magnitude limits much fainter than we require. These distributions are tabulated for 100 redshift bins, centered from $z_1 = 0.03$ to $z_2 = 1.47$ with spacing $dz = 1.44/99$. We find all the objects in our candidate isolated galaxy list which have a companion in the photoz2 catalogue satisfying the above projected separation and magnitude difference criteria, and we discard those where the companion has a photometrically estimated redshift distribution compatible with the spectroscopic redshift of the primary. Our definition of “compatible” is that the probability for the companion to have a redshift equal to or less than that of the primary exceeds 0.1. Apparent companions which fail this test usually do so because their colours are too red to be consistent with a redshift as low as that of the primary. After applying this additional cut, 41883 objects remain in our isolated galaxy sample.

Finally, we exclude any object for which more than 20% of a surrounding disc of radius $r_p = 1$ Mpc lies outside the survey footprint. Such objects could have bright companions which are not included in the SDSS databases. To evaluate these overlaps we made use of the set of “spherical polygons” provided on the NYU-VAGC website. These account both for the survey boundary and for masked areas around bright stars. We generate a large number of points uniformly and randomly over the 1 Mpc disc surrounding each galaxy and discard any which lie outside the survey boundary. A

galaxy is eliminated from the sample if more than 20% of its points are discarded in this way. This last cut removes about 1.5% of our objects, leaving a final sample of 41271 bright isolated galaxies. The set of randomly generated points surrounding each of these “primaries” is kept for later use when estimating background corrections to the counts of its faint companions (see below).

Figure 1 compares the distributions of colour, Petrosian half-light radius R_{50} , concentration $C = R_{90}/R_{50}$ and stellar surface mass density $\mu_* = M_*/2\pi R_{50}^2$ for our parent galaxy sample (all 145070 galaxies with $r < 16.6$) and for our 41271 isolated primaries, separated into bins of galaxy stellar mass. These quantities were taken directly from the NYU-VAGC catalogue. The stellar masses were estimated by fitting stellar population synthesis models to the K-corrected galaxy colours assuming a Chabrier (2003) initial mass function as in Blanton & Roweis (2007). The sensitivity of the stellar masses to assumptions underlying the estimation technique is explored in the Appendix of Li & White (2009). Each stellar mass bin is a factor of two wide, and we show data for the five mass bins on which we will concentrate our analysis throughout the rest of this paper. The numbers in the lower right of the R_{50} plots indicate the number of isolated primaries in each mass bin. Volume corrections have been applied to all the histograms in this figure by calculating the total volume V_{\max} of the survey over which each individual galaxy would be brighter than the flux limit, $r = 16.6$, and accumulating counts weighted by $1/V_{\max}$. It turns out that our isolated primaries are slightly bluer than the parent sample, particularly at low masses. In addition, they are slightly more concentrated than the parent sample. Our selection procedure appears to have no significant effect on the distributions of the other two properties, and the same is true for the redshift distributions which we do not show. To a very good approximation our isolated primary galaxies are typical objects of their stellar mass, although as we will see below, our selection has a strong influence on their relation to their environment. Vertical dashed lines in the colour plots indicate the split we adopt when separating our primaries into red and blue populations. This split is slightly dependent on stellar mass.

2.2 The mock catalogue

In the analysis and interpretation of our results for satellite galaxy populations we will make considerable use of mock catalogues built from the galaxy formation simulations of Guo et al. (2011, hereafter G11). These are implemented on two very large dark matter simulations, the Millennium Simulation (MS; Springel et al. 2005) and the Millennium-II Simulation (MS-II; Boylan-Kolchin et al. 2009). The MS follows the evolution of structure within a cube of side $500h^{-1}$ Mpc (comoving) and its merger trees are complete for subhaloes above a mass resolution limit of $1.7 \times 10^{10} h^{-1} M_\odot$. The MS-II follows a cube of side $100h^{-1}$ Mpc but with 125 times better mass resolution (subhalo masses greater than $1.4 \times 10^8 h^{-1} M_\odot$). Both adopt the same WMAP1-based Λ CDM cosmology (Spergel et al. 2003) with parameters $h = 0.73$, $\Omega_m = 0.25$, $\Omega_\Lambda = 0.75$, $n = 1$ and $\sigma_8 = 0.9$. These are outside the region preferred by more recent analyses (in particular, σ_8 appears too high) but this is of no consequence for the issues we study in this paper. For consis-

¹ <http://sdss.physics.nyu.edu/vagc/>

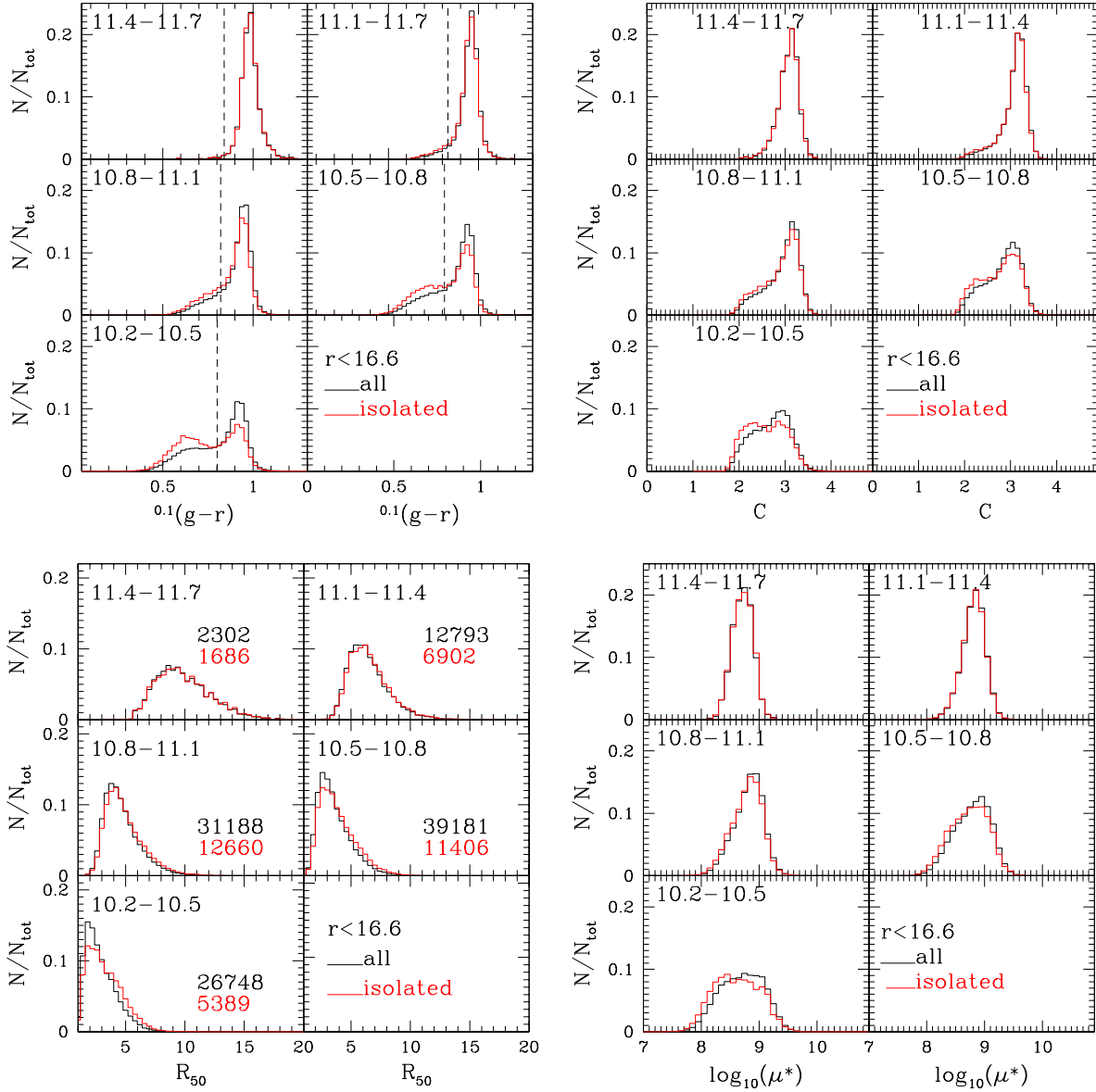


Figure 1. Volume weighted distributions for the parent sample of SDSS/DR7 galaxies with $r < 16.6$ (black curves) and for our sample of isolated galaxies (red curves). Different panels within each set refer to different ranges of $\log M_*/M_\odot$ as labelled. Each set corresponds to a different property. **Top left:** $^{0.1}(g-r)$ colour – the vertical dashed line in each panel shows the colour separating red and blue populations. **Top right:** Concentration $C = R_{90}/R_{50}$. **Bottom left:** Petrosian half-light radius R_{50} (in kpc) – the numbers at bottom right of each panel indicate the numbers of galaxies in the parent (black) and isolated samples (red) shown. **Bottom right:** Stellar surface mass density $\mu_* = M_*/2\pi R_{50}^2$.

tency, we will adopt this cosmology when quoting numbers in the rest of this paper.

In G11’s galaxy formation model, the uncertain star formation and feedback efficiencies are tuned to produce close fits to the stellar mass, luminosity and autocorrelation functions of low redshift galaxies as inferred from the SDSS. Together with their high resolution (particularly for the MS-II) and large volume (for the MS) this makes them ideal for our purposes in this paper. Here we use the publicly available data from <http://www.mpa-garching.mpg.de/millennium>. We project the simulation boxes in three orthogonal directions parallel to their x , y and z axes. In each projection

we can assign each galaxy a redshift based on its “line-of-sight” distance and peculiar velocity, and we can select isolated primaries using criteria which are directly analogous to those used for the SDSS (though we do not need to worry about the complications due to completeness and boundary issues). In addition to observables like luminosities, colours, sizes and morphologies, the simulation databases provide information which is not directly accessible for real galaxies (e.g. halo mass, environment type and full 3D position and peculiar velocity). These can give insight into the nature of the isolated primary sample we have selected.

All the SDSS luminosities and colours we use in this pa-

per are rest-frame quantities K-corrected to the $^{0.1}r$ band. The absolute magnitudes in our mock catalogues are in the true $z = 0$ r band, because this is what is directly provided by the database and the difference between the $^{0.1}r$ and r bands is too small to significantly affect luminosities. We do, however, transform the database ($g - r$) colours to the $^{0.1}(g - r)$ band using the empirical fitting formula of Blanton & Roweis (2007) because here the shifts seem large enough to cause (minor) differences.

Structure in the MS and MS-II is characterized using Friends-of-Friends (FoF) groups partitioned into sets of disjoint self-bound subhaloes. The subhalo populations at neighboring output times are linked to build merger trees which record the assembly history of all nonlinear structures and provide the framework for the galaxy formation simulations. In these simulations galaxy evolution is affected by environment in several ways. The galaxy at the centre of the most massive subhalo of each FoF group (which usually contains most of its mass) is considered the “central galaxy” and is the only one to accrete material from the diffuse gas associated with the group. When evolution joins two FoF groups, G11 continue to treat the galaxy at the centre of the less massive subhalo as a central galaxy until it falls within the nominal virial radius² of the new FoF group. After this point the infalling galaxy is considered as a “satellite”, the mass of its dark halo starts dropping as a result of tidal stripping, and its diffuse gas is assumed to be removed in proportion to the subhalo dark matter. Such satellites may later lose their subhaloes entirely through tidal disruption. At this point they are either disrupted themselves or (more commonly) they become “orphan satellites” which continue to orbit until dynamical friction causes a merger with their central galaxy. In this paper we will follow G11, considering together the two kinds of satellites (with and without a dark matter subhalo) and the two kinds of centrals (in dominant and in newly accreted, distant subhaloes).

The left panels of figure 2 compare halo mass distributions as a function of stellar mass for isolated simulation galaxies to those of their parent population. Here, halo mass is M_{200} of the FoF group for the dominant central galaxy and all the satellites, and M_{inf} for the other “centrals”, where M_{inf} is the M_{200} of the old FoF group of a newly accreted central just prior to infall. Our isolation criteria have a substantial effect on these mass distributions, eliminating a high-mass tail which is particularly evident for lower stellar mass galaxies. This tail is due to the satellites which, as we will show more explicitly below, are very effectively excluded by our criteria.

The right panels of figure 2 compare colour distributions for these same simulated galaxy populations. Just as for the real SDSS galaxies (figure 1) our isolation criteria bias the distributions to bluer galaxies because central galaxies have ongoing gas accretion and so are more actively star-forming than satellites. Selection induces larger shifts for the simulated distributions than for the real ones, however, and the bimodal nature of the colour distributions is more ob-

vious in the simulation. As already discussed by G11 and Weinmann et al. (2011) this reflects the facts that the red and blue sequences are more sharply defined in the simulation than in reality and that satellite galaxies appear to be too uniformly red. Note also that the red and blue populations separate at bluer colours (indicated by dashed vertical lines) in the simulation than in the SDSS data, particularly at high mass. This appears to be a consequence of the stellar population synthesis models used in the simulation, together with the fact that stellar metallicities are too low for high-mass galaxies (see Henriques & Thomas 2010).

The left panels of figure 3 illustrate how well our isolation criteria select central galaxies, at least in the simulation. The fraction of centrals according to the definitions of G11 is plotted as a function of stellar mass in the lower panel, with the black curve referring to all isolated galaxies and the red and blue curves referring to the red and blue subpopulations. For the isolated population as a whole and for its red subpopulation, the contamination by satellites *maximizes* at just over 2%. Slightly larger contamination occurs at high mass in the blue subpopulation, but such massive blue galaxies are in any case very rare (see below). In contrast, the curves in the upper panel show that only 65% of the parent population in the G11 model are centrals at $\log M_*/M_\odot = 10$, about 80% are centrals at $\log M_*/M_\odot = 11$ and 88% are centrals at $\log M_*/M_\odot = 11.5$. For blue galaxies the central fraction is above 90% at all masses, while for $\log M_*/M_\odot < 10.3$ most red galaxies are satellites. The application of our isolation criteria to the simulated galaxy population of G11 thus results in an extremely pure sample of central galaxies.

We cannot be sure, of course, that the elimination of satellite galaxies is as effective in the SDSS samples as in the simulation. We can, however, check that the separation into red and blue subpopulations matches as a function of stellar mass, both for isolated galaxies and for their parent population. This comparison is shown in the right panel of figure 3. Here red curves indicate the red fraction as a function of stellar mass for isolated galaxies, while black curves indicate the same quantity for the parent sample. In each case, solid curves are the observational result from SDSS and dashed curves are for the simulation of G11. For the observations we have again used $1/V_{\text{max}}$ weighting to ensure that the plotted quantity is appropriate for a volume-limited sample. For the primary stellar masses relevant for this paper ($\log M_*/M_\odot > 10.2$) the agreement between observation and simulation is almost perfect. At lower stellar masses there are too many red galaxies in the simulation, again reflecting the problem noted above and discussed in detail by Weinmann et al. (2011): at low masses the simulated satellite galaxies are too uniformly red.

Another comparison of the effects of our isolation criteria on the observed and simulated galaxy samples is shown in Figure 4. The thick black solid line here indicates, as a function of stellar mass, the fraction of galaxies from the parent sample which remain in our final sample of isolated SDSS galaxies. The thick black dashed line shows the result when analogous isolation criteria are applied to our G11 mock catalogues. The agreement of observation and simulation is again quite good, though not as perfect as in the right panel of figure 3. Note, however, that perfect agreement is not

² We define this as r_{200} the radius of the sphere centred on the gravitational potential minimum of the FoF group within which the mean density is 200 times the critical value. M_{200} is then the mass within this sphere.

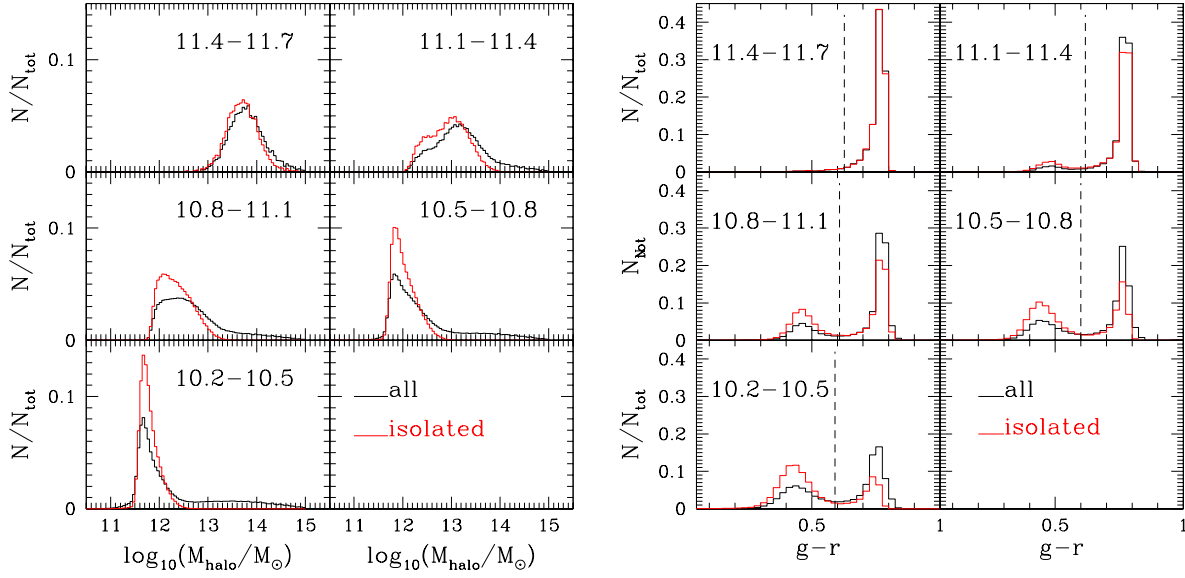


Figure 2. *Left:* Halo mass distributions for isolated galaxies (red curves) in five disjoint stellar mass bins and for the parent populations in the simulations of G11 from which they were drawn (black curves). *Right:* Colour distributions for these same sets of simulated galaxies. Vertical dashed lines indicate the colour at which we separate red and blue populations.

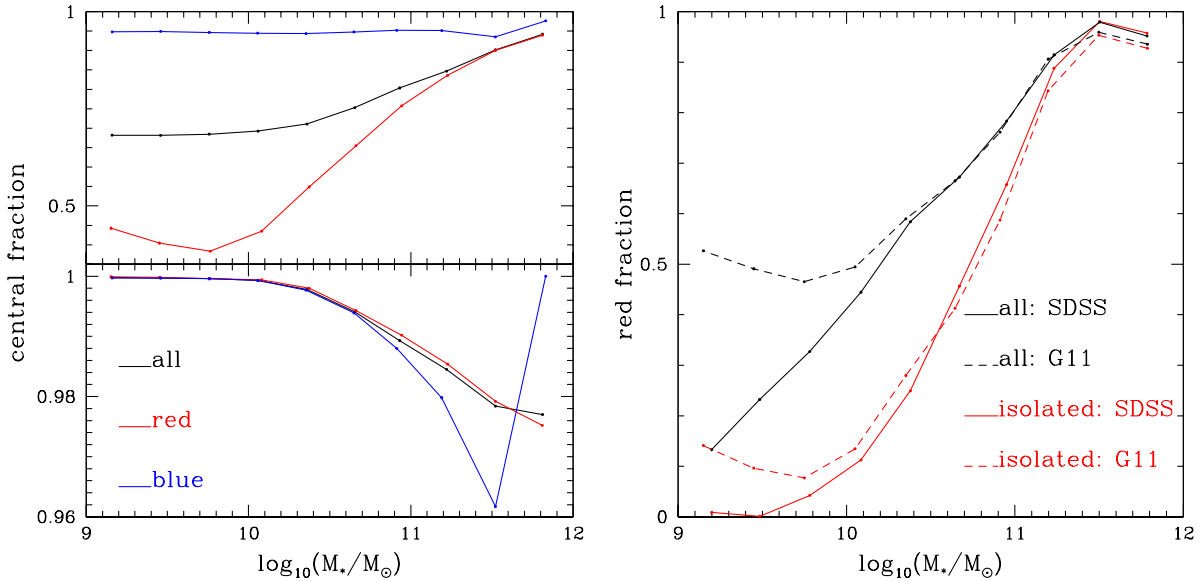


Figure 3. *Left:* The fraction of isolated galaxies (bottom panel) and of their parent sample of all galaxies (top panel) in the galaxy formation simulation of G11 which are classified as centrals rather than satellites according to the G11 criteria which we also adopt here (see the text for details). Black, red and blue lines indicate the fractions as a function of stellar mass for all, for red and for blue galaxies respectively. *Right:* The fractions of galaxies which are red (rather than blue) are shown as a function of stellar mass for isolated galaxies (red curves) and for the parent sample of all galaxies (black curves). The solid curves in each case represent observed results for the SDSS (after weighting to represent values for volume-limited samples) while the dashed curves are for the galaxies in the simulation of G11. Note the excellent agreement for $\log M_*/M_\odot > 10.2$ the range of interest for this paper.

expected, since the underlying SDSS sample is magnitude-limited whereas the G11 sample is volume-limited.

This same plot provides a convenient way to summarise the relative effects of the spectroscopic and photometric catalogues in defining our observed sample of isolated galaxies. The thin red solid line shows the fraction of objects

which are isolated relative to the spectroscopic sample, but not necessarily relative to the photometric sample. At most masses, use of the photometric catalogue increases the number of objects with an identified “companion” by 30 to 50%. This has a relatively small effect on the isolated fraction at high mass, since the great majority of massive galaxies are

isolated by our criteria. At $\log M_*/M_\odot = 10.3$ it reduces the number of isolated galaxies by almost a factor of two, however, because the majority of such SDSS galaxies have a companion by these same criteria. These numbers suggest (and we have checked in more detail) that our photometric rejection step is conservative, in that a significant fraction of the photometric “companions” (about one third) are, in fact, galaxies at a significantly different redshift which are projected on top of the primary. This does not matter for the analysis of this paper – it just causes us to end up with a slightly smaller sample of isolated primaries than if we had been less conservative.

Finally we can use the simulated catalogue to see how our isolation criteria affect the numbers of satellite and central galaxies in our samples. The green and blue dashed lines in Figure 4 show as a function of stellar mass the fractions of centrals and satellites which pass our isolation criteria. At high mass, most centrals are indeed isolated, but for $\log M_*/M_\odot < 10.6$ more than half of them are rejected because of apparent companions. In most cases these companions are actually the central galaxies of other haloes. On the other hand, for $\log M_*/M_\odot < 11$ almost all satellite galaxies are found to have companions according to our criteria. With increasing mass the number of apparently isolated satellites grows, reaching 30% at the highest mass. This is because these objects lie in very massive galaxy clusters and so can be projected more than 1 Mpc from their associated central galaxies. Note, however, that the actual number of such massive satellites is very small (see figure 3). It is the interplay of these different effects which produces the very high purity (i.e. central galaxy fraction) at all masses in our final isolated galaxy sample.

2.3 The photometric catalogue for satellites

Both the spectroscopic catalogue and the photoz2 photometric catalogue used in the last section are based on DR7, the seventh release of SDSS data. When identifying and verifying the isolation of our isolated primary galaxies, only objects with apparent magnitude brighter than $r = 17.6$ had to be considered. This is far above the magnitude limit of the SDSS photometry, and the accuracy of the DR7 magnitudes/colours and of the derived photo- z distributions is well tested at these magnitudes. When compiling counts of faint satellite galaxies around these primaries, we need to go to the SDSS limit for reliable photometry, however, which we take to be $r = 21$. At this limit, improvements to the photometry pipeline have continually enhanced its reliability, identifying (and correcting when possible) systematic artifacts which can have a significant influence on our analysis. We therefore use the photometric catalogue from SDSS/DR8³ (Aihara et al. 2011) when compiling satellite counts. To be specific we created a reference photometric catalogue by downloading objects that are classified as galaxies in the survey’s primary object list, and that do not have any of the flags BRIGHT, SATURATED, SATUR_CENTER or NOPETRO_BIG set. This follows the selection criteria for the DR7 photoz2 catalogue used above,

It is important to note that the magnitude we use for

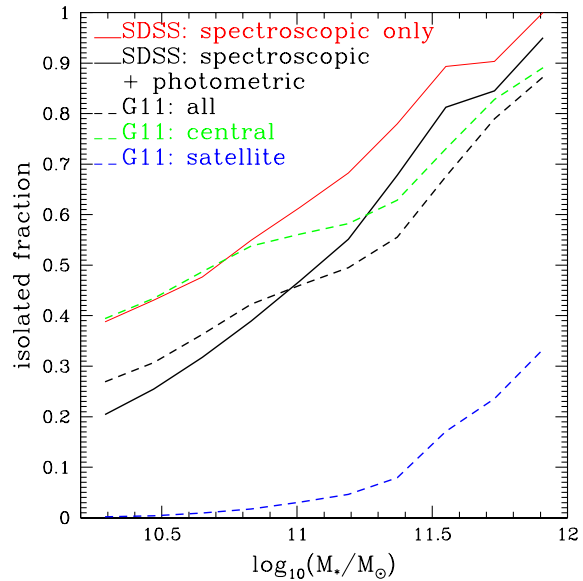


Figure 4. The fraction of galaxies that are selected by our isolation criteria as a function of stellar mass. The thick black solid line gives the result for our final sample of isolated SDSS galaxies, while the thick black dashed line is the corresponding result for simulated galaxies in the G11 model. These agree moderately well over the full mass range shown. The thin solid red line shows the fraction of retained SDSS galaxies after demanding isolation relative to the spectroscopic sample but before additionally requiring isolation relative to the photometric sample. Green and blue dashed curves indicate the fractions of central and satellite galaxies which remain after applying our isolation criteria to the G11 simulated galaxy sample.

satellites is the so-called SDSS model magnitude, which, at faint apparent magnitudes, is claimed to have the highest signal-to-noise of all the alternatives catalogued. In contrast, when defining our primary sample and checking its isolation we used Petrosian magnitudes as listed on the NYU-VAGC website. We continue to use these magnitudes for the primaries below. When we quote colours, these are always measured within a well-defined aperture related to the Petrosian radius, and are rest-frame quantities K-corrected to the $^{0.1}(g-r)$ band for both primaries and satellites. All absolute magnitudes quoted for SDSS galaxies are also in this same rest-frame band.

We have carried out a variety of tests for systematics in the SDSS photometry, checking completeness and the quality of star-galaxy separation by comparing with much deeper HST data, and quantifying systematic biases in the magnitudes of faint images (e.g. the satellites) in the neighborhood of substantially brighter images (e.g. the primaries). Detailed descriptions of these tests are given in an Appendix, along with details of tests of our procedures (outlined in the next section) for counting apparent companions around our primary galaxies and correcting for the (usually dominant) contribution from unrelated foreground and background objects.

³ <http://skyservice.pha.jhu.edu/casjobs/>

3 SATELLITE COUNTING METHODOLOGY

We want to study the abundance of satellites as a function of their luminosity, stellar mass and colour around our sample of isolated bright primaries, and to see how these abundances depend on the stellar mass and colour of the primary. We will need to use the SDSS data down to their reliable photometric limit (which we take to be $r = 21$) and as a result the great majority of the potential satellites do not have a spectroscopically measured redshift. Hence it is necessary to count *all* apparent neighbours around our primaries and to correct statistically for unassociated objects which happen to be projected near them. The number of such (mainly) background objects can substantially exceed the number of true satellites, so it is important to take considerable care in making these corrections. We adopt the following procedure.

For each isolated bright galaxy, we identify all photometric galaxies with apparent projected separation $r_p < 0.5$ Mpc and we accumulate counts in bins of projected separation r_p , apparent magnitude r and observed colour $g - r$. From the count in each $(r_p, r, g - r)$ bin, we subtract the expected number of background galaxies which we take to be $N(r, g - r)A(r_p, z)/A_{\text{tot}}$, where $N(r, g - r)$ is the total number of galaxies in the $(r, g - r)$ bin in the full photometric catalogue, A_{tot} is the solid angle of the survey footprint, $A(r_p, z_{\text{pri}})$ is the solid angle corresponding to the annular r_p bin at the redshift z_{pri} of the primary galaxy, and f is the incompleteness factor, the fraction of this annulus which lies within the survey footprint (we estimate this using the random points generated around the position of each primary during the selection process – see above). We then use the redshift of the primary galaxy to convert observed apparent magnitudes and colours into rest-frame luminosities and colours (in the $^{0.1}r$ and $^{0.1}(g - r)$ system)⁴ and we transfer the background-subtracted satellite counts from our narrow bins of r and $g - r$ into substantially broader bins of the rest-frame quantities. Finally we average these counts for each r_p bin over the set of all primaries in the desired range of stellar mass (and sometimes colour) and we sum the result over the desired range in r_p . Uncertainties in the resulting numbers are estimated from the scatter among results for 100 bootstrap resamplings of the set of primaries.

Some apparent companions are too red to be at the redshift of the primary galaxy. It is useful to exclude them when accumulating counts since they add noise without adding signal. Hence, we exclude all bins redder than $^{0.1}(g - r) = 0.032 \log_{10} M_{\star} + 0.73$, a fit to the upper envelope of the distribution of rest-frame colour against stellar mass for galaxies of measured redshift. The stellar mass M_{\star} of the apparent companion is estimated by assuming it to be at the primary's redshift and adopting

$$(M/L)_r = -1.0819^{0.1}(g-r)^2 + 4.1183^{0.1}(g-r) - 0.7837 \quad (1)$$

This empirical relation is a fit to a flux-limited ($r < 17.6$) galaxy sample from the NYU-VAGC website for which stellar masses were estimated from the K-corrected galaxy colours by fitting stellar population synthe-

sis models assuming a Chabrier (2003) initial mass function (Blanton & Roweis 2007). For this sample the $1\text{-}\sigma$ scatter in $(M/L)_r$ of this simple relation is about 0.1.

The photometric catalogue we use is complete down to an r -band apparent model magnitude of 21. This limit corresponds, of course, to different satellite luminosities and stellar masses for different primary redshifts and different satellite colours. In order to ensure that our samples are complete when compiling satellite luminosity functions, we allow a particular primary to contribute counts to a particular luminosity bin only if the K-corrected absolute luminosity corresponding to $r = 21$ for a galaxy at the redshift of the primary and lying on the red envelope of the intrinsic colour distribution is fainter than the lower luminosity limit of the bin. Thus only the nearest primaries will contribute to the faintest luminosity bins of our satellite luminosity functions, and different numbers of primaries will contribute to each bin. We follow an exactly analogous procedure when compiling stellar mass functions for satellites.

For each individual satellite luminosity/stellar mass bin, this treatment is equivalent to imposing an upper limit on primary redshift. Thus there is a maximum volume which is surveyed for satellites in the j th luminosity/stellar mass bin which we denote $V_{\text{max}, \text{bin}, j}$.

On the other hand, our primary sample is flux-limited at $r = 16.6$, so for brighter satellite bins where $V_{\text{max}, \text{bin}, j}$ is large, intrinsically faint primaries will not be visible to the redshift limit. The effective volume surveyed is then $V_{\text{max}, \text{pri}, i}$, the total survey volume over which the i th primary would lie above the flux limit. Note that because of K-corrections, this volume depends on the intrinsic colour of the primary as well as its intrinsic luminosity. We present our final results in the form of the mean number of satellites per primary for a volume-limited primary sample

$$N_{\text{sat}, j} = \frac{\sum_i N_{\text{sat}, i, j} / V_{\text{max}, ij}}{\sum_i 1 / V_{\text{max}, ij}}, \quad (2)$$

where

$$V_{\text{max}, ij} = \min[V_{\text{max}, \text{pri}, i}, V_{\text{max}, \text{bin}, j}]. \quad (3)$$

Thus, for satellite luminosity/stellar mass bin j , we sum satellite counts over all primaries i that are within $V_{\text{max}, \text{bin}, j}$. At the bright end of the satellite luminosity function, we expect $V_{\text{max}, ij} = V_{\text{max}, \text{pri}, i}$ because satellites are less than 4.4 magnitudes fainter than their primaries and so can be seen around all primaries. For intrinsically faint satellites, however, $V_{\text{max}, ij} = V_{\text{max}, \text{bin}, j}$ because primaries can be seen to well beyond the distance at which $r = 21$ for the satellites.

We apply similar selection criteria to our mock catalogues based on G11. Since we know the absolute magnitude, rest-frame colour and stellar mass of all galaxies, the background subtraction can be carried out directly using rest-frame quantities. In addition, the effective depth of the satellite catalogue is the same for all primaries so that all primaries can contribute to all satellite luminosity or stellar mass bins and we do not need any weighting in order to obtain proper volume-weighted statistics. Note that we do not use any information about the redshift difference between primary and apparent companion, so projection effects occur over $\Delta z = 50,000$ km/s corresponding to the side of the Millennium Simulation “box”. Both for the simulation and for the real SDSS data we use a global background estimate

⁴ We use the empirical fitting formula of Westra et al. (2010) which gives the K-correction as a function of redshift and observed colour.

based on the full survey in order to minimize the statistical uncertainty in the correction.

Previous work often estimated a background density locally for each primary (e.g. Lorrimer et al. 1994; Guo et al. 2011). This not only substantially increases the noise, it also introduces a significant bias since galaxies are correlated on all scales and the “background” fields are, in fact, expected to have faint galaxy densities significantly above the mean. The extent of the bias is, in fact, strongly dependent on the isolation criteria and can be of either sign (see, for example, Fall et al. 1976). The large-scale uniformity of the SDSS photometry is such that there appears to be no advantage to adopt a local estimate, provided all photometric quantities are properly corrected for Galactic extinction. The accuracy of our method is confirmed by the accurate convergence to unity at large angular scale in the left panel of figure A1 and by a variety of tests which we describe in detail in the Appendix.

4 LUMINOSITY AND MASS FUNCTIONS OF SATELLITE GALAXIES

4.1 Luminosity functions

In figure 5 we present $^{0.1}r$ -band luminosity functions for satellites projected within 300 kpc of their primaries, except for the faintest bin, where the halo virial radius is much smaller than 300 kpc and we estimate the luminosity function within 170 kpc in order to increase the signal-to-noise. In the left panel, data points connected by solid lines show our observational results for SDSS/DR8. As indicated in the legend, colours encode the range in $\log M_*/M_\odot$ of the primaries contributing to each luminosity function estimate. Error bars are derived by bootstrap resampling the primary sample. At the faint end we lose higher redshift primaries because of the apparent magnitude limit of our photometric catalogue. We do not plot data for bins with fewer than eight primaries. It is evident that satellite numbers increase strongly with primary mass.

The black solid line in the left panel shows a Schechter (1976) function fit to the data for the most massive primaries. We have fixed the characteristic luminosity and faint-end slope to be those of the SDSS field luminosity function in $^{0.1}r$ (Montero-Dorta & Prada 2009). The result is a moderately good fit to the satellite data, although these appear steeper than the field luminosity function at the faintest magnitudes. The satellite luminosity functions clearly become steeper for lower mass primaries. Power-law fits to the faint-end data are shown as dashed lines in the figure and give the slopes α listed in the first row of table 1. The bright end of each function is cut off by our requirement that every satellite be at least one magnitude fainter than its primary. We therefore exclude one or two of the brightest points when making these fits. Specifically, we find the median absolute magnitude M_{med} for primaries in each mass range, and we include only points for which the corresponding absolute magnitude bin lies entirely below $M_{\text{med}}+1$. The ranges fitted in each case are indicated by the extents of the dashed black straight lines.⁵ The faint-end slope decreases

⁵ We have checked that the remaining points are indeed unaf-

ected by $\alpha \sim -1.2$ for $\log M_{*,p}/M_\odot \sim 11.5$ to $\alpha \sim -1.6$ for $\log M_{*,p}/M_\odot \sim 10.3$.

Guo et al. (2011) divided their primaries into three luminosity ranges ($M_r = -23.0 \pm 0.5$, -23.0 ± 0.5 and -23.0 ± 0.5) and compiled satellite luminosity functions in bins of satellite-primary magnitude difference rather than satellite absolute magnitude. They quote faint-end slopes of -1.45, -1.725 and -1.96 for these three sets of primaries, with the fainter primaries having steeper luminosity functions. For the largest measured magnitude differences ($\Delta m \sim 8$) they found similar numbers of satellites independent of primary luminosity. These α values are substantially more negative than ours, particularly for the faintest primaries. In order to compare with their results, we adopt similar isolation criteria, we take the same ranges of primary luminosity, and we also accumulate satellite number as a function of magnitude difference. Fitting the faint-end slope over the same satellite magnitude range as in figure 7 of Guo et al. (2011), we find α values of -1.189, -1.376 and -1.588, substantially shallower than those of Guo et al. (2011) and quite compatible with those we quote in Table 1. Detailed tests show this inconsistency to be due partly to the local background subtraction scheme of Guo et al. (2011) which removes part of the signal⁶, but mainly to the fact that they use model magnitudes K-corrected to $z = 0$ for their primaries, rather than the $^{0.1}r$ Petrosian magnitudes which we use here.

In the right panel of figure 5, the small symbols joined by solid lines show analogous results for the galaxy formation model of G11, based on the Millennium and Millennium-II simulations. Points brighter than $M_r = -18$ are MS data. At fainter magnitudes, resolution effects cause the MS to underestimate galaxy abundances and we take our data from the MS-II. (The two simulations agree very well in the range $-18 > M_r > -20$.) To facilitate comparison, we replot the SDSS data from the left panel as filled triangles. Agreement of model and observation is fair but far from perfect. The simulation overpredicts the number of satellites around the most massive primaries by 25 to 50% for $M_r > -19.5$. In the two lower primary stellar mass ranges, the simulation underpredicts the number of satellites by 20 to 30%. As we will see below, the latter discrepancy reflects a problem with the colours of the simulated satellites rather than with their stellar masses. The black dashed lines in this panel are the “field” luminosity function for the full simulations renormalized to fit the satellite data for each primary mass range. Here also there is a trend for the faint-end slope to be steeper for satellites than in the field, but the effect is much less marked than for the SDSS data. Furthermore the

affected by rebinning our data as a function of the r -band absolute magnitude of the primaries. In this case we know exactly which bins are unaffected by our isolation criterion. When primary absolute magnitude and stellar mass are matched appropriately, the resulting satellite luminosity functions match those of figure 5 very closely over the full range used to determine the faint-end slope and are unaffected by the isolation criterion over this range.

⁶ Guo et al. (2011) used photometry from SDSS/DR7 while our own tests, similar to those discussed in section A1 of the Appendix, showed to suffer from substantially more serious systematics for faint images close to brighter ones than is the case for the SDSS/DR8 catalogues used here.

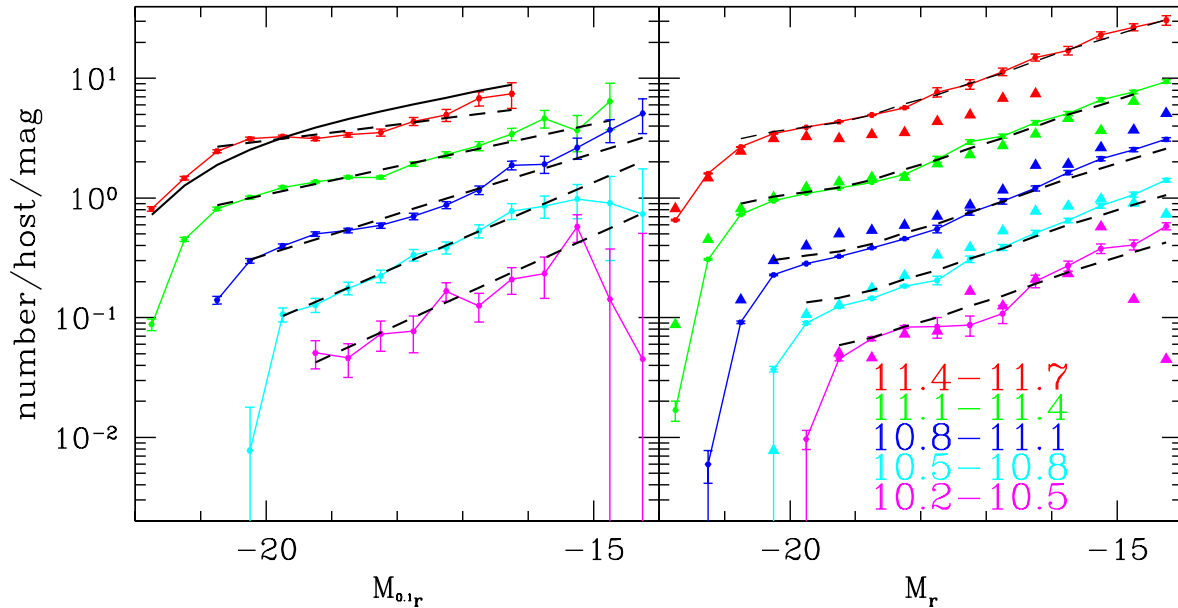


Figure 5. Luminosity functions in the $0.1r$ band for satellites of primary galaxies in five disjoint ranges of $\log M_*/M_\odot$, as indicated in the legend. Satellites are counted within a projected radius of 300 kpc, except for the lowest mass range where we count within 170 kpc. In the left panel, the data points connected by solid lines give observational results for SDSS/DR8 with error bars estimated by bootstrap resampling of the primary sample. The solid black line is a fit of a Schechter (1976) function to the most massive bin, with the characteristic luminosity and faint-end slope constrained to match those of the SDSS field luminosity function. Dashed black lines are power-law fits excluding one or two of the brightest points for each mass range, as indicated by the line extent (see the text). In the right panel, the small symbols connected by solid lines show corresponding results for the G11 simulated galaxy populations. Black dashed lines here show the mean luminosity function for all simulated galaxies, renormalized to fit the satellite data as in the left panel. The SDSS results are overplotted as filled triangles for ease of comparison.

Table 1. Exponent α of the faint-end-slope for SDSS luminosity and mass functions

Range in primary $\log M_*/M_\odot$	11.7-11.4	11.1-11.4	10.8-11.1	10.5-10.8	10.2-10.5
Luminosity function	-1.170	-1.295	-1.424	-1.587	-1.622
Mass function	-1.231	-1.297	-1.455	-1.800	-1.748

variation of faint-end slope with primary mass seen in the SDSS is weak or absent in the simulation data.

Many previous papers have investigated the shape and faint-end slope of group/cluster luminosity functions (e.g. Paolillo et al. 2001; Goto et al. 2002; Christlein & Zabludoff 2003; De Propris et al. 2003; Andreon, Punzi, & Grado 2005; Popesso et al. 2005, 2006; Zandivarez, Martínez, & Merchán 2006; Hansen et al. 2009; Alshino et al. 2010; de Filippis et al. 2011). Unfortunately there is little consensus. Some authors found large differences between cluster and field luminosity functions, while others found the two to be quite similar. For example, by stacking SDSS data around the centres of clusters detected in the Rosat All Sky Survey, Popesso et al. (2006) obtained cluster luminosity functions with a very obvious steepening at faint magnitudes. This faint-end upturn appeared to be contributed primarily by early-type galaxies. In our most massive primary stellar mass bin ($11.7 > \log_{10} M_* > 11.4$), there is qualitatively similar behaviour with an upturn at

$M_r \sim -18$ as in Popesso et al. (2006) but the steepening is much less dramatic in our data than in theirs. In contrast, no evidence of an upturn at the faint end was found by Alshino et al. (2010) and de Filippis et al. (2011) in galaxy clusters.

4.2 Stellar mass functions

Figure 6 is similar to figure 5, but shows stellar mass functions for satellites both in the SDSS (left panel) and in the G11 simulations (right panel with the SDSS data repeated as filled triangles). The strong dependence of satellite number on primary mass is again evident. The black solid line overplotted on the most massive bin is a Schechter function fit with characteristic mass and low-mass slope fixed to the “field” values of Li & White (2009). The observed satellite stellar mass functions are again steeper than the corresponding field functions at the low-mass end. The black

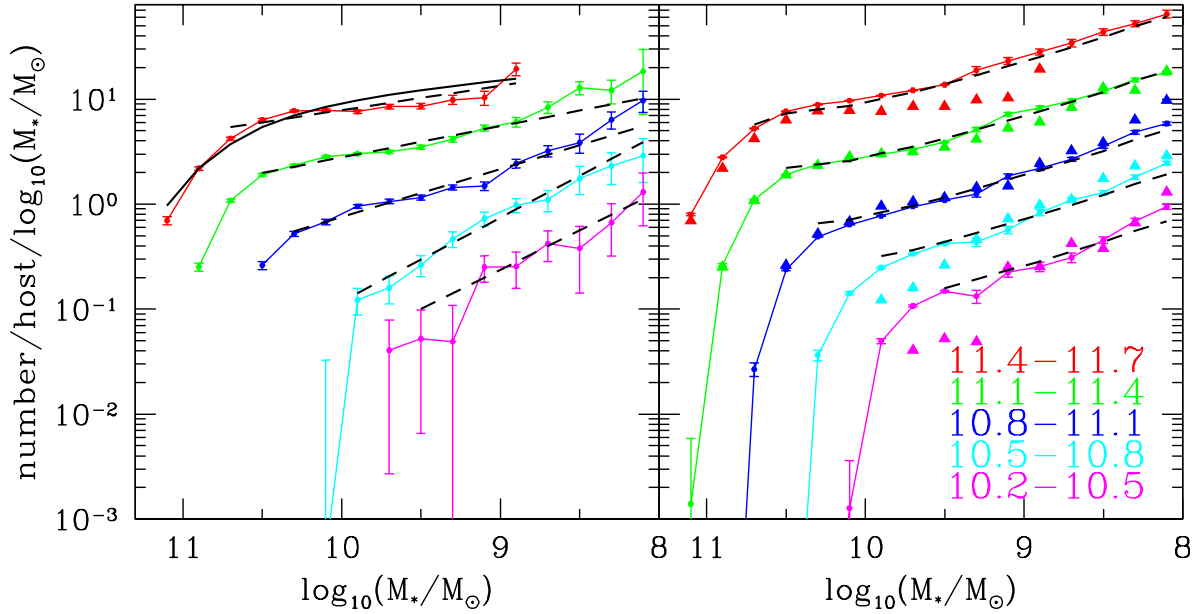


Figure 6. Similar to figure 5 but showing stellar mass functions for satellites projected within 300 kpc (or 170 kpc) of their primaries, both for the SDSS (left panel) and for the G11 simulations (right panel with the SDSS data repeated as filled triangles). As in figure 5, the primaries are grouped into five disjoint ranges of $\log M_*/M_\odot$, as indicated by the colours. A black solid line in the left panel is a renormalized version of the “field” stellar mass function of Li & White (2009) overplotted on the data for the highest mass primaries, while dashed black lines show a power law fit to each mass function estimate. In the right panel the dashed black lines are fits of the satellite data to renormalized versions of the stellar mass function of the simulation as a whole.

dashed lines in the left panel are power-law fits to the observational data. The corresponding faint-end-slopes are given in the second row of table 1. Here also we have ignored the few brightest points in each estimate. As before the extent of each dashed black line indicates the points actually used in the fit. The steepening of the satellite stellar mass functions with decreasing primary mass is even stronger than was the case for the satellite luminosity functions.

In the right panel of figure 6, the G11 points are taken from the MS at $\log M_*/M_\odot > 9.5$ and from the MS-II at lower mass. Fits to the field stellar mass function from the simulations are shown as dashed lines and indicate no significant shape difference between the two. Comparison with the SDSS data shows that the overprediction of the satellite luminosity function for the most massive primaries persists in very similar form in their stellar mass function, The underprediction found for the two lower primary mass ranges has gone away, however, indicating that the discrepancy was due primarily to the colours of the simulated satellites, rather than to their stellar masses. The simulation does not reproduce the clear steepening of the SDSS satellite mass functions with decreasing primary mass. Any effect in this direction is very weak.

To investigate further the origin of the observed steepening with decreasing primary mass, we take all spectroscopic galaxies brighter than 16.6 in the r -band, without applying any isolation criterion, and calculate the mass function of surrounding satellites within 300 (or 170) kpc in exactly the same way as for our isolated primaries. Results are shown as solid curves in figure A6. In this case there is

no steepening with decreasing primary mass – the different colour curves are more or less parallel to each other and to the field stellar mass function. Apparently, the steepening is caused by our isolation criteria – isolated galaxies have fewer lower mass neighbours than typical galaxies. The suppression is stronger for more massive neighbours, steepening the satellite mass functions of isolated primaries. Notice that for primaries with $\log M_*/M_\odot > 10.8$, the mean numbers of low-mass companions are similar for isolated and for typical objects, but that lower mass primaries have substantially fewer such companions if they are isolated. This is because many of the lower mass non-isolated “primaries” are, in fact, satellites themselves, and their low-mass “companions” are fellow satellites within the larger system. It is quite interesting that the abundance of relatively small satellites is strongly affected by the presence or absence of a nearby galaxy comparable in luminosity to the primary, particularly since the observed trends are not fully reproduced by the simulation. This suggests that dwarf galaxy formation may be influenced by nearby giants in a way which the simulation does not represent.

It is interesting to see whether satellite galaxy populations depend on the colour of the primary galaxy as well as on its stellar mass. Figures 7 and 8 show the satellite mass functions surrounding red and blue primaries respectively, where the primary populations have been split at the colours indicated in figures 1 and 2. The black dashed lines in the left panels are power-law fits, but in each case the slope is fixed to be that found for all primaries in the relevant stellar mass bin (table 1). In the right panel of figure 8

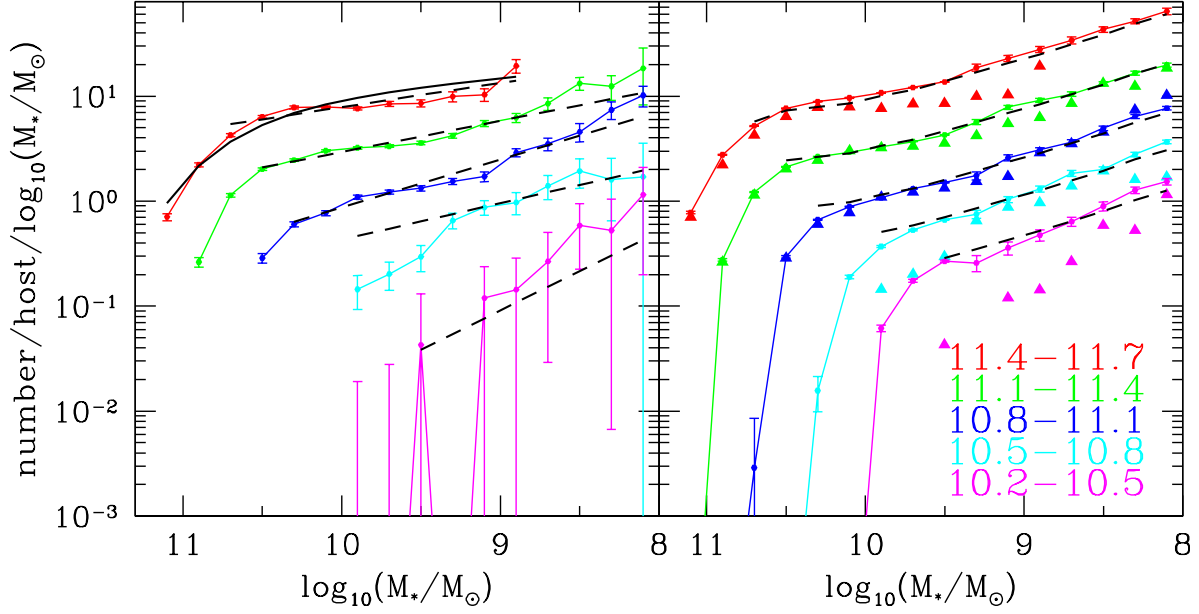


Figure 7. Similar to figure 6, but for red primaries. See figures 1 and 2 for the colour cuts separating red and blue primaries.

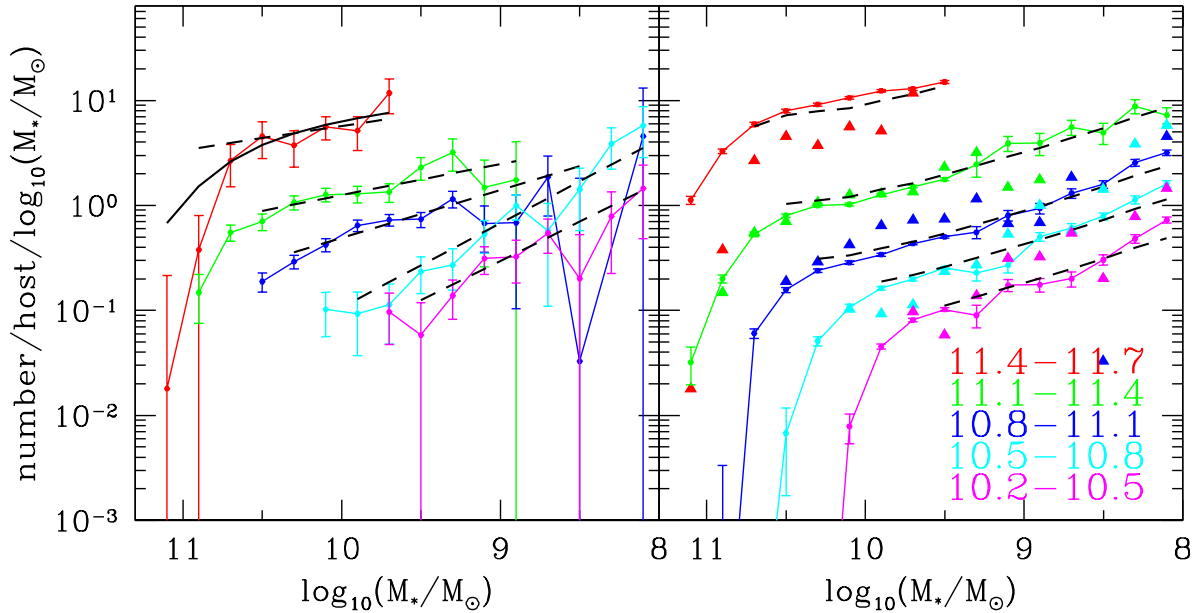


Figure 8. Similar to figure 6, but for blue primaries. In the right panel, the red dots connected by a curve stop at $\log_{10} M_* = 9.5$, because the Millennium-II Simulation has fewer than eight blue primaries more massive than $\log_{10} M_* / M_{\odot} = 11.4$.

the red curve stops at $\log M_* / M_{\odot} = 9.5$ because the MS-II contains fewer than eight blue primaries more massive than $\log M_* / M_{\odot} = 11.4$ and the MS population is affected by numerical resolution at lower satellite mass. For red primaries the SDSS and G11 data agree quite well, apart from the slope discrepancy and a residual overprediction of the abundance of faint satellites around high-mass primaries. For

blue primaries, the differences are bigger but in the highest mass bin this could reflect the small number of SDSS primaries and the correspondingly large observational error bars. The discrepancy for primaries in the stellar mass range $10.1 > \log M_* / M_{\odot} > 10.8$ is smaller but more significant, particularly since there is good agreement in this mass range for red primaries. Interestingly, a comparison of figures 7

and 8 shows that the amplitude of the satellite luminosity function is higher around red primaries than around blue primaries of the same stellar mass. We analyze this result in more detail in the following subsections.

4.3 Satellite abundance as a function of primary stellar mass and colour

In order to better display how the abundance of satellites depends on the stellar mass and colour of the primary, we use the power-law fits shown as dashed lines in figures 6, 7 and 8 to predict the mean number of satellites per primary in the stellar mass range $10.0 > \log M_*/M_\odot > 9.0$ and at projected separation $r_p < 300$ kpc ($r_p < 170$ kpc for the lowest mass primaries). This has the advantage of producing a robust measure of satellite abundance which is little affected either by selection-induced cut-offs (most important for low-mass and red primaries) or by incompleteness (most important for high-mass and blue primaries). The results are shown in the left panels of figure 9, where black dots and lines give results for all primaries, while red and blue dots and lines give results for red and blue primaries, respectively. The top panel presents results for the SDSS and the lower panel results for the G11 simulations. The SDSS result for all primaries is repeated in the lower panel, showing that the simulation overpredicts the number of satellites in this mass and projected radius range both for the highest mass and for the lowest mass primaries. Note that because the low-mass slopes differ in simulation and observation, the result for low-mass primaries depends on the satellite mass range chosen for the comparison.

At high mass the black and red curves in figure 9 are close to each other, reflecting the fact that the fraction of red primaries is large (see figure 3). At the highest mass, the blue curve indicates a consistent number of satellites around blue primaries, although with considerable uncertainty because such primaries are rare. At somewhat lower mass, however, blue primaries have significantly fewer satellites than red primaries *of the same stellar mass*, both in the SDSS data and in the simulation. This is a primary result of our paper. The effect is a factor of two to three in satellite abundance for primaries with $\log M_*/M_\odot \sim 11$. In the SDSS data there is some indication that the colour dependence may get smaller again for lower mass primaries, but this does not happen in the simulation, where there is still more than a factor of two difference for $M_* \sim 2 \times 10^{10} M_\odot$. Overall, the differences appear somewhat larger in the model than in the real data.

The cause of this effect in the G11 simulation is easy to track down. In the right-hand panels of figure 9 we plot histograms of host halo mass for isolated galaxies as a function of their stellar mass and colour. (As shown in figure 3, almost all isolated galaxies in the simulation are the central galaxies of their haloes.) For all except the highest stellar mass range, red primaries have significantly more massive dark haloes than blue ones. The shift between the peaks of the two distribution is an order of magnitude for primaries with $11.4 > \log M_*/M_\odot \sim 11.1$, dropping to a factor of two for $10.5 > \log M_*/M_\odot \sim 10.2$. In the simulation red primaries have more satellites because they live in more massive haloes. A direct indication that the same may hold for real galaxies comes from the galaxy-galaxy lensing study of

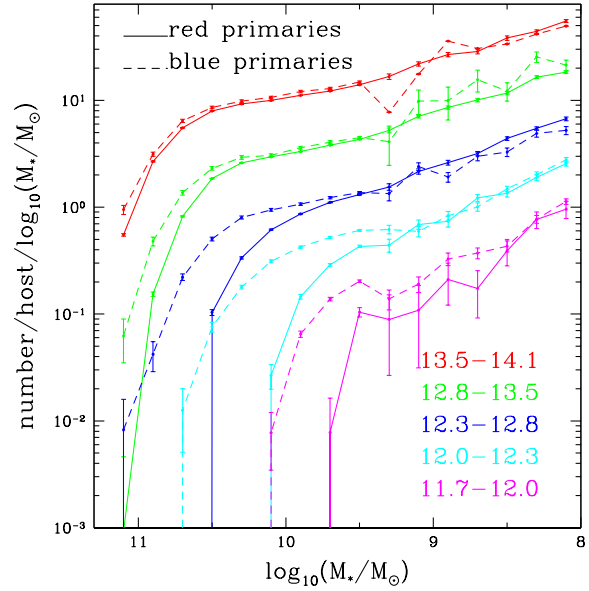


Figure 10. Satellite mass functions within $r_p = 300$ kpc, split according to *halo* mass, for dark haloes in the G11 galaxy formation simulation. The colours refer to different ranges of $\log M_{\text{halo}}/M_\odot$ as indicated in the legend. For each halo mass range, satellite stellar mass functions are shown separately for haloes with red (solid lines) and blue (dashed lines) central galaxies.

Mandelbaum et al. (2006). By combining their SDSS lensing data with HOD modeling, these authors concluded that red galaxies have more massive haloes than blue ones for $\log M_*/M_\odot > 11$. At lower central galaxy masses their results appear consistent with no offset, although the error bars are large (see their figure 4).

The fact that both the number of satellites and the mass of the associated dark halo depend not only on the stellar mass of the primary galaxy but also on its colour contradicts the assumptions underlying many HOD or abundance matching schemes for interpreting large-scale galaxy clustering. Such a dependence could be included in more complex versions of at least the former, but would require additional parameters and additional observational data to constrain them (e.g. Simon et al. 2009; Ross & Brunner 2009; Skibba & Sheth 2009).

Within the simulation it is possible to check whether halo mass is the only factor responsible for the difference in satellite abundance between red and blue primaries. In figure 10 we present stellar mass functions for satellites of isolated galaxies as a function of the *halo* mass of the primary. As before these are compiled for satellites projected within $r_p = 300$ kpc. The halo mass ranges for this plot are chosen to correspond roughly to the primary stellar mass ranges in previous figures. For each halo mass range, the mass functions are also split according to the colour of the primary galaxy, with solid and dashed lines referring to results for red and blue primaries respectively. At low satellite mass there is excellent agreement between the solid and dashed curves, indicating that satellite abundance does not depend on central galaxy colour at fixed halo mass. For the most massive haloes there are few blue primaries in the MS-II, so the red dashed curve is quite noisy below $\log M_*/M_\odot = 9.5$. For

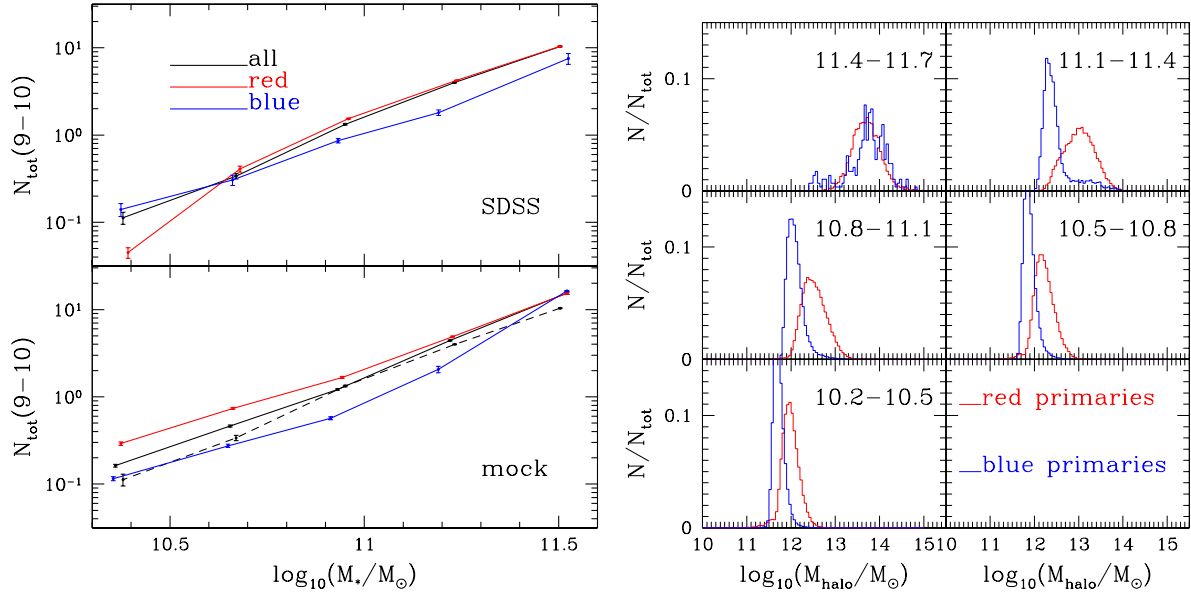


Figure 9. *Left:* Mean number of satellites in the stellar mass range $10.0 > \log M_*/M_\odot > 9.0$ as a function of primary stellar mass. Black, red and blue points refer to all, to red and to blue primaries, respectively. For the points at lowest primary mass, satellite counts were accumulated within 170 kpc, whereas for all other primary masses they were accumulated within 300 kpc. The top panel gives observational results for the SDSS while the bottom panel gives corresponding results for the G11 galaxy formation simulations. The SDSS result for all primaries is re-plotted as a dashed curve in the bottom panel in order to facilitate comparison. *Right:* Host halo mass distributions for red and blue primaries in the simulated catalogues, split into the same primary stellar mass ranges as in the left-hand plots.

massive satellites there are obvious discrepancies between the dashed and solid curves, but these result from our sample definition. At given halo mass, red primaries have smaller stellar masses and so substantially lower luminosities than blue ones. Our isolation criteria then imply a correspondingly lower upper limit on the stellar mass of satellites for the red primaries. The effect is largest for the lowest mass haloes.

Sales et al. (2007) used the galaxy formation simulation of Croton et al. (2006), also based on the Millennium Simulation, to study the relation between primary luminosity/stellar mass and satellite velocity dispersion, which should be a good diagnostic of halo mass. Although they found a strong dependence of velocity dispersion on galaxy colour at fixed primary luminosity, this dependence almost vanished at fixed primary stellar mass. This appears to contradict our results from the G11 simulation. At $\log M_*/M_\odot \sim 11$, where we find the biggest difference in satellite abundance between red and blue primaries, almost a factor of three, the difference in velocity dispersion in their figure 13 is at most 20%, corresponding to a factor of at most 1.7 in halo mass (since $M_h \propto \sigma^3$). The discrepancy could result from the different isolation criteria adopted in the two studies, from departures from a straightforward relation between 3-D velocity dispersion within r_{200} (the quantity considered by Sales et al. (2007)), halo mass and projected satellite count within 300 kpc (the quantity considered here), or from differences between the two galaxy formation models.

So far we have characterized the abundance of satellites by the count within $r_p = 300$ kpc (or $r_p = 170$ kpc for the lowest mass bin in figure 9) In order to better understand

the relation with halo mass, it is useful instead to consider the count within the virial radius of the haloes, which we define as r_{200} , the radius of a sphere within which the mean mass density is 200 times the critical value. We obtain such a measure using the equation,

$$N(r < r_{200}) = N_p(r_p < 300 \text{ kpc}) \times \frac{M(r < r_{200})}{M_p(r_p < 300 \text{ kpc})}, \quad (4)$$

where M_p and N_p are projected quantities and M and N the corresponding 3-dimensional quantities. The projected abundance $N_p(r_p < 300 \text{ kpc})$ is taken directly from figure 9, and we calculate the mass ratio on the *rhs* of equation 4 assuming an NFW profile. The halo radius r_{200} is known for each simulated galaxy, but can only be inferred indirectly for the SDSS objects. We assume that the mean halo mass at given stellar mass is the same in the observations as in the G11 simulations. The mass ratio also depends weakly on halo concentration which we take from the model of Zhao et al. (2009).

For each primary stellar mass bin in figure 9 we can then estimate a mean halo mass $\langle M_{200} \rangle$. We take the mean satellite number per primary given by equation 4 and divide by this mean halo mass to obtain the abundance per unit halo mass of satellites in the stellar mass range $10.0 > \log M_*/M_\odot > 9.0$. Finally, we divide this quantity by the abundance per unit (total) mass of galaxies in this same stellar mass range in the Universe as a whole, taken from Li & White (2009) for the SDSS data and from the G11 simulation as a whole for the mock data. The result is a measure of the formation efficiency of low-mass galaxies as a function of their present environment, as characterized by mass of the halo in which they live. Figure 11 shows this efficiency as a function of mean halo mass for all primaries

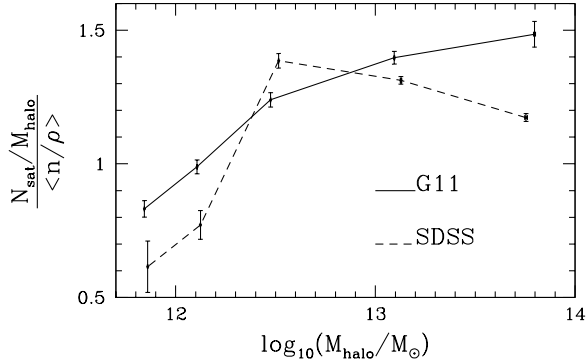


Figure 11. Mean number of satellites in the stellar mass range $10.0 > \log M_*/M_\odot > 9.0$ per unit total halo mass, relative to the mean abundance per unit total mass of such galaxies in the Universe as a whole. Isolated primary galaxies are grouped into the same five stellar mass bins used in figure 9. Results for the G11 simulations and for the SDSS are shown by solid and dashed curves respectively. The mean halo mass has been calculated directly for each bin in the simulation data. Each SDSS primary is assigned a halo mass using the simulation relation between mean halo mass and primary stellar mass for all primaries. This plot hence shows the efficiency of low-mass galaxy formation as a function of present-day halo mass in units of the overall efficiency in the Universe as a whole.

in the five stellar mass bins of figure 9. There are three significant points to take from this plot: (i) the formation efficiency of low-mass satellite galaxies varies rather little with the mass of the halo in which the galaxies are found today; (ii) in massive haloes this efficiency is about 50% larger than the efficiency for forming such galaxies in the universe as a whole (remember that, globally, about half the galaxies in this stellar mass range are satellites); (iii) finally there is fair agreement between the formation efficiencies in the simulation and in the real universe, although this is in part due to our use of the simulation to assign halo masses to the observed galaxies.

5 SATELLITE COLOUR DISTRIBUTIONS

So far we have studied the abundance of satellites as a function of the stellar mass and colour of their primary and as a function of their own luminosity and stellar mass. In this section we study how the *colours* of satellite galaxies depend on the properties of their primaries. Figures 12 and 13 show cumulative colour distributions for satellites in the SDSS and in the G11 catalogues respectively, as a function of the stellar mass and colour of their primary. The distributions are for satellites in two different stellar mass ranges, as indicated by the labels above the relevant panels, and refer to all satellites projected within 300 kpc. The top, middle and bottom panels in each column refer to satellites of all, of red and of blue primaries respectively, while the different colours of the curves in each panel encode the stellar mass range of the primary galaxies. The black curves which repeat in all the panels of each column give the colour distributions for field galaxies in the same stellar mass range as the satellites (calculated for SDSS from all galaxies in the

NYU-VAGC with $r < 17.6$, and for G11 from all galaxies within the simulation volume). The dashed horizontal line is merely a reference to facilitate identification of the median colour.

A number of systematic trends are evident in these plots. Concentrating first on the observational results in figure 12, we see that more massive primaries have redder satellites within 300 kpc (in every panel the curves are ordered cyan-blue-green-red from top to bottom), that low-mass satellites are bluer than high-mass ones (the curves in the right panels are always bluer than the corresponding curves in the left panels), satellites are systematically redder than field galaxies of the same mass, except possibly for the lowest mass primaries (the coloured curves almost always lie below the corresponding black curves), and red primaries have redder satellites than blue primaries of the same stellar mass (every coloured curve in the lowest panels is bluer than the corresponding curve in the middle panel). This last trend is the “galactic conformity” effect pointed out by Weinmann et al. (2006).

If we now compare with the simulation results in figure 13 we see that the same four systematic trends are present. More massive primaries have redder satellites; lower mass satellites are bluer; satellite galaxies are redder than field galaxies of the same stellar mass; and red primaries have redder satellites than blue primaries of the same stellar mass. However, there is an obvious discrepancy in that simulated satellites are systematically redder than observed satellites. This is true for all primary and satellite masses, but is particularly marked for lower mass and red primaries, and for lower mass satellites. Clearly, the theoretical model of G11 suppresses star formation much more effectively in such satellites than is the case in the real universe. This echoes the conclusions of Weinmann et al. (2006) about the earlier models of De Lucia & Blaizot (2007). The excessive reddening of the simulated satellite population reduces but does not eliminate all the other trends mentioned above.

The galactic conformity phenomenon has been discussed in a number of previous publications (e.g. Weinmann et al. 2006; Ann, Park, & Choi 2008; Kauffmann, Li, & Heckman 2010; Prescott et al. 2011). Weinmann et al. (2006) showed that, among groups of given luminosity (which they considered a proxy for halo mass), those with an early-type central galaxy have a larger fraction of early-type satellites. They considered several physical processes which might be responsible for this (halo and/or galaxy mergers, ram-pressure stripping, strangulation, harassment...), focusing on whether these processes could alter galaxy morphology. However, as discussed in some detail by Kauffmann et al. (2004) and re-emphasized in the context of galactic conformity by Kauffmann, Li, & Heckman (2010), it is important to separate star formation activity, stellar mass and galaxy structure when analyzing the influence of environment on galaxy properties. Typical classifications into “early” and “late” types mix aspects of all of these. The conformity effects we see here are for given central galaxy stellar mass (rather than luminosity), are within a fixed projected radius (300 kpc), and refer specifically to the *colours* of satellites and primaries. It seems possible that they could be due at least in part to the tendency for red centrals to have more massive haloes than blue ones, together with the trends

for satellites to get redder with increasing halo mass and decreasing r/r_{200} .

This can be checked directly for the simulated galaxy catalogues of G11. In figure 14 we again show cumulative satellite colour distributions for two different satellite mass ranges and for all, for red and for blue primaries, but now in bins of host halo mass rather than of primary stellar mass. In this plot, the colour distributions are calculated for all satellites projected within the halo virial radius rather than for a fixed projected radius of 300 kpc. The halo mass ranges have been chosen to correspond approximately to the primary stellar mass ranges we have been using in previous plots. For the two high-mass bins, the colour distributions show no significant dependence on the colour of the central galaxy, but for the two low-mass bins the dependence on primary colour, while smaller than in figure 13, is clearly still present. Thus there must be physical processes in the model which contribute to the “galactic conformity” phenomenon in addition to those which result in red primaries having more massive haloes than blue primaries of the same stellar mass.

We have analyzed our simulation to identify candidates for these additional processes. In figures 15 and 16 we plot distributions for the two which show the strongest trends. Figure 15 shows the distributions of black hole mass and of hot gas mass for haloes in these same four mass ranges, split according to the colour of the central galaxy. Figure 16 shows similar plots for the cumulative distributions of infall redshift (defined as the redshift when a satellite last entered the virial radius r_{200} of the main progenitor of its halo) for satellites with stellar mass above $10^9 M_\odot$. In all cases the distributions depend strongly on central galaxy colour for haloes in the two lower mass ranges where galactic conformity effects are substantial, but at most weakly for higher mass haloes where these effects are absent. For $\log M_h/M_\odot < 12.8$, haloes with red central galaxies have more hot gas, more massive central black holes and earlier satellite infall redshifts than haloes of the same mass with blue central galaxies. Notice that the black hole mass distribution for blue centrals is bimodal in the lower left panel of figure 15. Clearly, there is a transition in this halo mass range between blue centrals with high-mass black holes (about 0.3% of their stellar mass, as in the upper panels) and blue centrals with low-mass black holes (roughly an order of magnitude smaller as a fraction of stellar mass, as in the lower right panel). The hot gas fractions are similar to the overall cosmic baryon fraction ($\sim 17\%$) for haloes with red central galaxies and about a factor of two smaller in the lower mass haloes with blue centrals. The transition halo mass is approximately the mass at which both observational and simulated samples of isolated galaxies become dominated by red objects (see figure 3).

Given the modeling assumptions of G11, these systematic differences mean that, for $\log M_h/M_\odot < 12.8$, haloes with red central galaxies have gas cooling rates which are twice but “radio mode” heating rates which are 20 times those of similar mass haloes with blue central galaxies. Thus, their central galaxies are clearly red because feedback has quenched their growth, and this is why their stellar masses are smaller than those of the blue centrals which have continued to grow to the present day. The redness of the satellite population in haloes with red centrals can be traced to

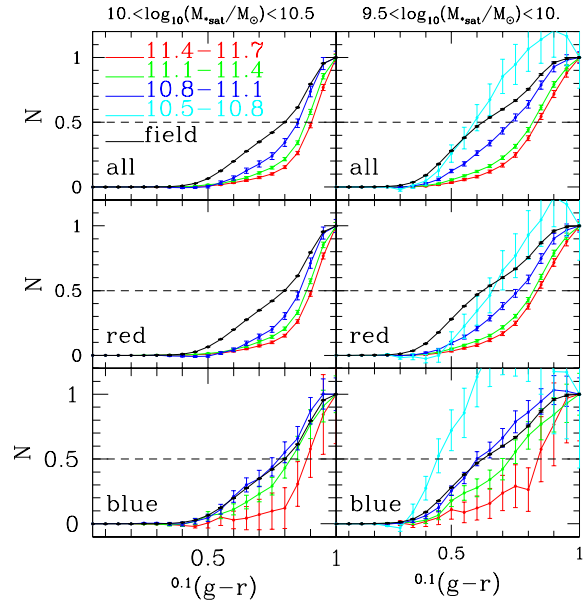


Figure 12. Cumulative colour distributions for satellites projected within 300 kpc of their primary as a function of primary stellar mass (indicated by line colour) for two ranges of satellite mass (left and right columns with the range indicated by the label above each column) and for all, for red and for blue primaries (upper middle and lower panels in each column). Black lines show the cumulative colour distribution for a volume-limited sample of field galaxies derived from the SDSS DR7 spectroscopic sample with $r < 17.6$.

the facts that the satellites are accreted earlier and orbit through a denser hot gas medium. Thus both tidal and ram pressure stripping processes are more effective, and the satellites have had longer to exhaust any remaining star-forming gas. Finally, the earlier assembly indicated by the higher satellite infall redshifts presumably explains why these particular haloes have red centrals, bigger black holes and more hot gas.

Thus, at least in the models, it is clear why there is galactic conformity at given halo mass. The more easily observable galactic conformity at given central stellar mass is predicted to be stronger as a result of the combination of these effects with the tendencies for red centrals to have more massive haloes at given stellar mass than blue ones, and for more massive haloes to have redder satellites. Yet stronger conformity effects are expected at given central galaxy luminosity, since blue central galaxies have smaller stellar masses (and thus even smaller halo masses) than red central galaxies of the same luminosity.

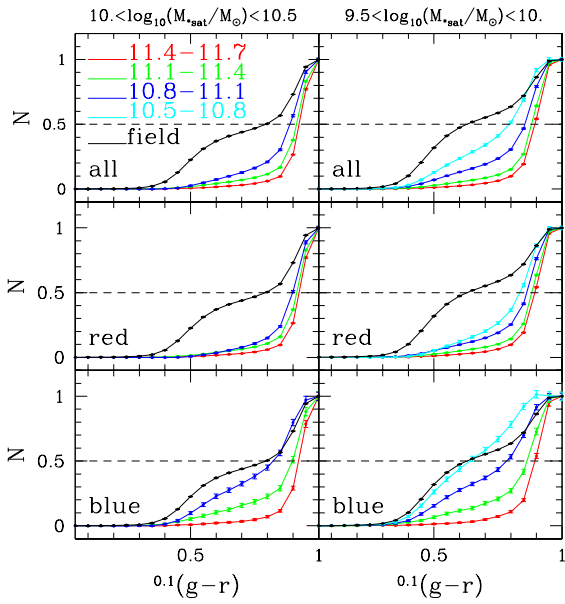


Figure 13. Similar to figure 12, but for the simulated galaxy catalogues of G11. The black lines here are the colour distributions for all galaxies in the specified stellar mass ranges within the full simulation volume.

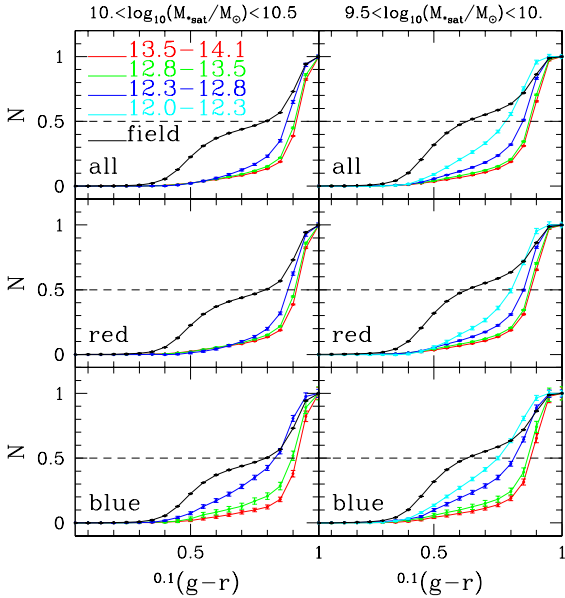


Figure 14. Colour distribution of satellites projected within the halo virial radius r_{200} of all primaries, of red primaries and of blue primaries (top, middle and bottom rows) as a function of host halo mass (indicated by line colours corresponding to the ranges of $\log M_h/M_\odot$ given in the legend) in the simulated galaxy catalogues of G11. Results are again shown for two ranges of satellite stellar mass.

6 SUMMARY AND CONCLUSIONS

We have used a photometric catalogue of SDSS/DR8 galaxies brighter than $r = 21$ to study the satellite populations of 41271 isolated galaxies with $r < 16.6$ selected from the SDSS/DR7 spectroscopic catalogue. In particular, we have studied how the abundance of satellites as a function of

luminosity, stellar mass and colour depends on the stellar mass and colour of the central galaxy. Our study differs from other recent SDSS-based studies of satellite galaxies (Lares, Lambas, & Domínguez 2011; Guo et al. 2011) in the size of the sample analyzed, in our primary focus on systematics as a function of stellar mass, and in our detailed comparison with the predictions of simulations of the evolution of the galaxy population in the concordance Λ CDM cosmology. In general, our results confirm and extend those obtained earlier, but the comparison with simulations allows us to identify the likely physical cause of most of the effects we see, and to isolate those which do not have a natural explanation within our current theory of galaxy formation.

Our observational samples and analysis procedures allow us to measure the properties of the satellite population in an unbiased way down to absolute magnitudes $M_{0.1r} \sim -14$ and stellar masses $\log M_*/M_\odot \sim 8$. Our main observational conclusions are as follows:

- Satellite luminosity and stellar mass functions have shapes consistent with those of the general field galaxy population only around the highest stellar mass primaries $\log M_*/M_\odot > 11.4$. These are all brightest cluster galaxies. For lower mass primaries, these functions become progressively steeper, even after accounting for the bright-end cut-off induced by our isolation criteria. This steepening is more marked for the stellar mass functions than for the luminosity functions because observed satellites get bluer as their stellar mass decreases.

- The mean abundance of satellites increases strongly with primary stellar mass, approximately as expected if the number of satellites is proportional to dark halo mass.

- For $\log M_*/M_\odot > 10.8$, red primaries have more satellites than blue primaries of the same stellar mass. The effect exceeds a factor of two for $\log M_*/M_\odot \sim 11.2$. This is reminiscent of the result of Mandelbaum et al. (2006) who showed that at high stellar mass, red central galaxies have more massive haloes than blue ones. This trend could in part be due to colour dependent errors in deriving stellar masses from the photometry, but such errors would need to be quite large and to depend on primary mass.

- Satellite galaxies are systematically redder than field galaxies of the same stellar mass except around blue primaries with $\log M_*/M_\odot < 10.8$ where the satellites can have similar colours or even be systematically bluer than the field (i.e. the galaxy population within a large representative volume).

- The satellite population is systematically redder around more massive primaries, for more massive satellites and around red primaries. The first effect reflects the fact that cluster galaxies are systematically redder than field galaxies, the second echoes the trend found in the general field, and the third is the galactic conformity effect pointed out by Weinmann et al. (2006) but measured here for fixed central stellar mass rather than fixed central luminosity.

We used criteria directly analogous to those employed on the SDSS to construct an isolated galaxy sample from the $z = 0$ output of the publicly available galaxy formation simulations of Guo et al. (2011, G11). These are based on the Millennium and Millennium-II Simulations. The mock catalogue contains similar magnitude, stellar mass, colour and position/velocity information to the real catalogue, but

also contains information about dark haloes and the location of the galaxies within them. Based on the mock sample, we conclude that $\sim 98\%$ of our isolated galaxies are the central objects of their dark haloes. Both in the SDSS and in the mock catalogue, the distributions of intrinsic properties for the isolated and parent populations are very similar. Only the colour distributions shift slightly, with the isolated galaxies being systematically bluer than the full population. A detailed comparison of the mock and real samples leads to the following conclusions

- At all primary masses, the luminosity and stellar mass functions of G11 satellites are quite similar both in shape and in normalization to those measured for SDSS. However, in the simulation there is only a weak tendency for the satellite functions to be steeper than those of the field, or to be steeper for lower mass primaries. This disagrees with the SDSS where the steepening with decreasing primary mass is quite marked.

- In the mock catalogues the abundance of satellites increases with primary stellar mass almost in proportion to mean halo mass. For high-mass haloes, the abundance per unit mass of satellite galaxies is about 1.5 times the value for the universe as a whole.

- For $\log M_*/M_\odot < 11.4$, red simulated primaries have more satellites than blue ones of the same stellar mass. The effect is similar in strength to that seen in SDSS but continues to lower primary mass. In the simulation it is due entirely to red primaries having more massive haloes than blue ones. At fixed *halo* mass the abundance of faint satellites is independent of the colour of the primary, but red primaries have lower stellar masses because of their truncated star formation histories.

- Satellite galaxies in the G11 simulations are systematically redder than in the SDSS. The effect is particularly marked for lower mass satellites and around lower mass primaries. The modeling improvements introduced by G11 to address this issue are apparently insufficient to fully solve it. Star formation is still terminated too early when galaxies become satellites.

- Despite this overall shift, the colours of simulated satellites depend on the colour and stellar mass of their primary and on their own stellar mass in very similar ways as in the SDSS. Satellites are systematically redder if they are more massive, if their primary is more massive, and if their primary is red. The first trend echoes that found for field galaxies, while the second reflects the fact that more massive haloes contain redder satellites. The third trend, the galactic conformity effect, is caused by redder primaries having more massive haloes at fixed stellar mass, and denser hot gas atmospheres (hence more effective ram-pressure stripping) at fixed halo mass.

Satellites go red in the G11 simulations because they lose their source of new cold gas. Once they fall within the virial radius of their host, their hot gas reservoirs are gradually removed by tidal and ram-pressure stripping and no new material is added by infall. Star formation uses up the remaining cold gas and then switches off. Clearly this happens too quickly (see Weinmann et al. (2011) and also Wang et al. (2007) for an explicit demonstration of how lengthening the relevant timescales can cure the problem) so improving the model will require changing the star for-

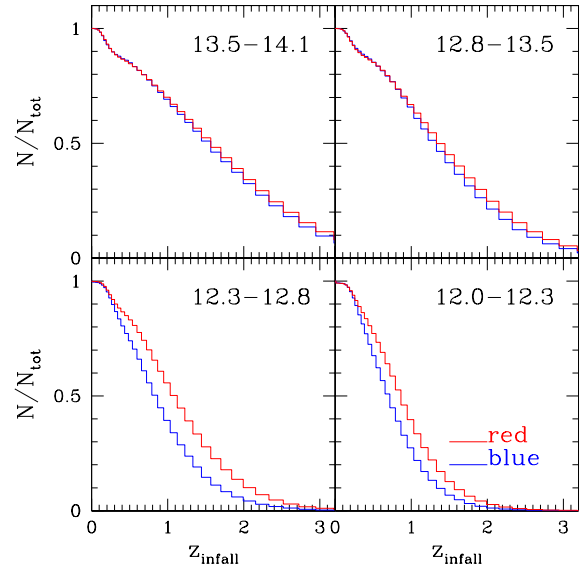


Figure 16. Infall time distributions for satellites in the same four ranges of halo mass used in figure 14 and again split according to the colour of the central galaxy.

mation assumptions to increase the time to gas exhaustion (for example, by removing the threshold gas surface density for star formation) or providing new sources of fuel (for example, by including the gas return from stellar evolution). Once this is fixed, it seems likely that the other trends of satellite colour with environment will be well matched.

The other clear discrepancy between the SDSS data and the simulation is the steepening of satellite mass and luminosity functions as one goes to fainter primaries. This is a relatively strong effect in the real data (and is visible also in the analysis of Guo et al. (2011)) but does not occur at a significant level in the simulations. Thus, it must reflect not merely the statistics of hierarchical clustering in a Λ CDM cosmology, but in addition some difference in the star-formation histories of satellite galaxies living in different mass host haloes. This may be related to the discrepancy noted by G11 – comparisons with high-redshift data suggest that low-mass galaxies form too early in their simulations – but this can only be checked by further simulation work. It is clear that the detailed and relatively precise statistical information provided by large-sample studies of satellite galaxies is useful for testing and refining our understanding of how galaxies form. In a follow-up paper we will extend our current study by considering satellite galaxy properties as a function of distance from the primary,

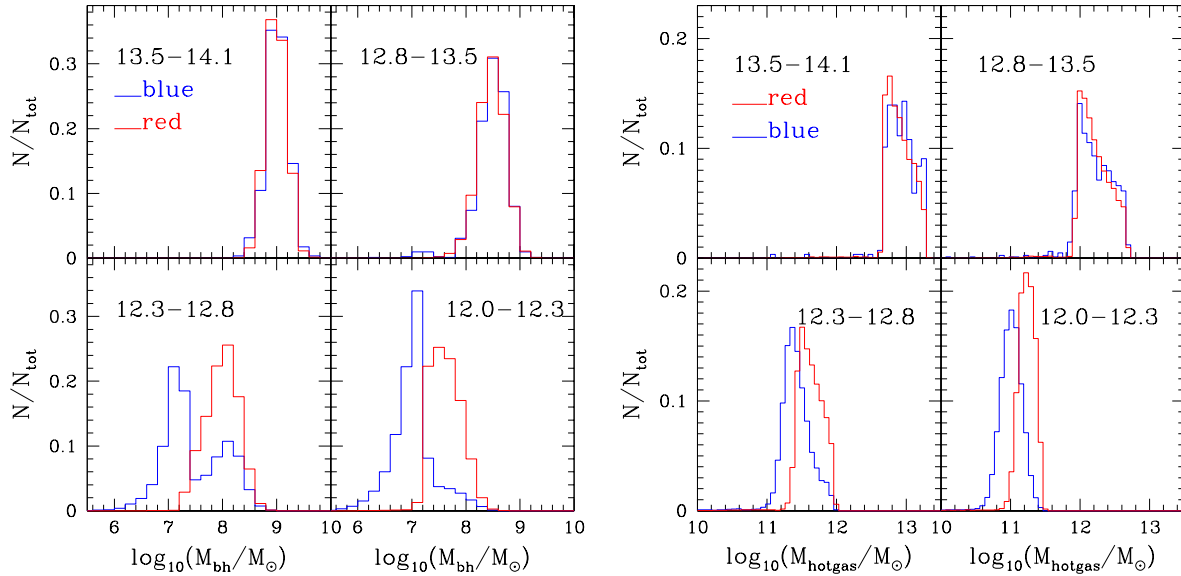


Figure 15. **Left:** Central black hole mass distributions for the same four ranges of halo mass used in figure 14 and split according to the colour of the central galaxy. **Right:** Hot gas mass distributions for the same four sets of haloes and again split according to the colour of the central galaxy.

ACKNOWLEDGEMENTS

We gratefully thank Rachel Mandelbaum for useful discussions about SDSS systematics, Xu Kong for supplying the COSMOS mask and Cheng Li for discussions about details of the NYU-VAGC and photoz2 catalogues. Wenting Wang is partially supported by NSFC (11121062, 10878001, 11033006, 11003035), and by the CAS/SAFEA International Partnership Program for Creative Research Teams (KJXC2-YW-T23).

REFERENCES

- Abazajian K. N., et al., 2009, *ApJS*, 182, 543
 Aihara H., et al., 2011, *ApJS*, 193, 29
 Alshino A., Khosroshahi H., Ponman T., Willis J., Pierre M., Pacaud F., Smith G. P., 2010, *MNRAS*, 401, 941
 Andreon S., Punzi G., Grado A., 2005, *MNRAS*, 360, 727
 Ann H. B., Park C., Choi Y.-Y., 2008, *MNRAS*, 389, 86
 Benson A. J., Frenk C. S., Lacey C. G., Baugh C. M., Cole S., 2002, *MNRAS*, 333, 177
 Berlind, A. A., Weinberg, D. H. 2002. The Halo Occupation Distribution: Toward an Empirical Determination of the Relation between Galaxies and Mass. *The Astrophysical Journal* 575, 587-616.
 Blanton M. R., et al., 2005, *AJ*, 129, 2562
 Blanton M. R., Roweis S., 2007, *AJ*, 133, 734
 Bode P., Ostriker J. P., Turok N., 2001, *ApJ*, 556, 93
 Bower R. G., Benson A. J., Malbon R., Helly J. C., Frenk C. S., Baugh C. M., Cole S., Lacey C. G., 2006, *MNRAS*, 370, 645
 Boylan-Kolchin M., Springel V., White S. D. M., Jenkins A., Lemson G., 2009, *MNRAS*, 398, 1150
 Boylan-Kolchin M., Springel V., White S. D. M., Jenkins A., 2010, *MNRAS*, 406, 896
 Boylan-Kolchin M., Bullock J. S., Kaplinghat M., 2012, *MNRAS*, 422, 1203
 Boylan-Kolchin M., Bullock J. S., Kaplinghat M., 2011, *MNRAS*, 415, L40
 Bullock J. S., Kravtsov A. V., Weinberg D. H., 2000, *ApJ*, 539, 517
 Capak P., et al., 2007, *ApJS*, 172, 99
 Chabrier G., 2003, *PASP*, 115, 763
 Chen J., Kravtsov A. V., Prada F., Sheldon E. S., Klypin A. A., Blanton M. R., Brinkmann J., Thakar A. R., 2006, *ApJ*, 647, 86
 Christlein D., Zabludoff A. I., 2003, *ApJ*, 591, 764
 Cole S., Aragon-Salamanca A., Frenk C. S., Navarro J. F., Zepf S. E., 1994, *MNRAS*, 271, 781
 Conroy C., et al., 2005, *ApJ*, 635, 982
 Conroy C., et al., 2007, *ApJ*, 654, 153
 Conroy C., Wechsler R. H., Kravtsov A. V., 2006, *ApJ*, 647, 201
 Cooray A., Sheth R., 2002, *PhR*, 372, 1
 Croton D. J., et al., 2006, *MNRAS*, 365, 11
 Cunha C. E., Lima M., Oyaizu H., Frieman J., Lin H., 2009, *MNRAS*, 396, 2379
 De Lucia G., Blaizot J., 2007, *MNRAS*, 375, 2
 De Propris R., et al., 2003, *MNRAS*, 342, 725
 Driver S. P., et al., 2009, *A&G*, 50, 050000
 Driver S. P., et al., 2011, *MNRAS*, 413, 971
 de Filippis E., Paolillo M., Longo G., La Barbera F., de Carvalho R. R., Gal R., 2011, *MNRAS*, 414, 2771
 Fall S. M., Geller M. J., Jones B. J. T., White S. D. M., 1976, *ApJ*, 205, L121
 Ferrero I., Abadi M. G., Navarro J. F., Sales L. V., Gurovich S., 2011, *arXiv*, arXiv:1111.6609
 Font A. S., et al., 2011, *MNRAS*, 417, 1260
 Goto T., et al., 2002, *AJ*, 123, 1807
 Grebel E. K., 2000, *ESASP*, 445, 87
 Grebel E. K., 2001, *ApSSS*, 277, 231

- Grebel E. K., 2007, *gnu.conf*, 3
- Grebel E. K., 2011, *EAS*, 48, 315
- Guo Q., White S., Li C., Boylan-Kolchin M., 2010, *MNRAS*, 404, 1111
- Guo Q., et al., 2011, *MNRAS*, 413, 101
- Guo Q., Cole S., Eke V., Frenk C., 2011, *MNRAS*, 417, 370
- Hansen S. M., Sheldon E. S., Wechsler R. H., Koester B. P., 2009, *ApJ*, 699, 1333
- Henriques B. M. B., Thomas P. A., 2010, *MNRAS*, 403, 768
- Henriques B. M. B., White S. D. M., Lemson G., Thomas P. A., Guo Q., Marleau G.-D., Overzier R. A., 2012, *MNRAS*, 421, 2904
- Holmberg E., 1969, *ArA*, 5, 305
- Jing Y. P., Mo H. J., Boerner G., 1998, *ApJ*, 494, 1
- Jing Y. P., Boerner G., 1998, *ApJ*, 503, 37
- Kauffmann G., White S. D. M., Guiderdoni B., 1993, *MNRAS*, 264, 201
- Kauffmann G., Colberg J. M., Diaferio A., White S. D. M., 1999, *MNRAS*, 303, 188
- Kauffmann G., White S. D. M., Heckman T. M., Ménard B., Brinchmann J., Charlot S., Tremonti C., Brinkmann J., 2004, *MNRAS*, 353, 713
- Kauffmann G., Li C., Heckman T. M., 2010, *MNRAS*, 409, 491
- Kang X., Jing Y. P., Mo H. J., Börner G., 2005, *ApJ*, 631, 21
- Klypin A., Kravtsov A. V., Valenzuela O., Prada F., 1999, *ApJ*, 522, 82
- Koposov S., et al., 2008, *ApJ*, 686, 279
- Koposov S. E., Yoo J., Rix H.-W., Weinberg D. H., Macciò A. V., Escudé J. M., 2009, *ApJ*, 696, 2179
- Kravtsov A. V., Gnedin O. Y., Klypin A. A., 2004, *ApJ*, 609, 482
- Lacey C., Cole S., 1993, *MNRAS*, 262, 627
- Lares M., Lambas D. G., Domínguez M. J., 2011, *AJ*, 142, 13
- Li C., White S. D. M., 2009, *MNRAS*, 398, 2177
- Liu L., Gerke B. F., Wechsler R. H., Behroozi P. S., Busha M. T., 2011, *ApJ*, 733, 62
- Lorrimer S. J., Frenk C. S., Smith R. M., White S. D. M., Zaritsky D., 1994, *MNRAS*, 269, 696
- Lovell M. R., et al., 2012, *MNRAS*, 420, 2318
- Ma C.-P., Fry J. N., 2000, *ApJ*, 543, 503
- Macciò A. V., Kang X., Fontanot F., Somerville R. S., Koposov S., Monaco P., 2010, *MNRAS*, 402, 1995
- Mandelbaum R., et al., 2005, *MNRAS*, 361, 1287
- Mandelbaum R., Seljak U., Kauffmann G., Hirata C. M., Brinkmann J., 2006, *MNRAS*, 368, 715
- Mandelbaum R., Seljak U., Cool R. J., Blanton M., Hirata C. M., Brinkmann J., 2006, *MNRAS*, 372, 758
- Montero-Dorta A. D., Prada F., 2009, *MNRAS*, 399, 1106
- Moore B., Ghigna S., Governato F., Lake G., Quinn T., Stadel J., Tozzi P., 1999, *ApJ*, 524, L19
- Moore B., Gelato S., Jenkins A., Pearce F. R., Quilis V., 2000, *ApJ*, 535, L21
- More S., van den Bosch F. C., Cacciato M., Skibba R., Mo H. J., Yang X., 2011, *MNRAS*, 410, 210
- Moster B. P., Somerville R. S., Maulbetsch C., van den Bosch F. C., Macciò A. V., Naab T., Oser L., 2010, *ApJ*, 710, 903
- Navarro J. F., Frenk C. S., White S. D. M., 1996, *ApJ*, 462, 563
- Navarro J. F., Frenk C. S., White S. D. M., 1997, *ApJ*, 490, 493
- Nierenberg A. M., Auger M. W., Treu T., Marshall P. J., Fassnacht C. D., Busha M. T., 2012, *ApJ*, 752, 99
- Paolillo M., Andreon S., Longo G., Puddu E., Gal R. R., Scaramella R., Djorgovski S. G., de Carvalho R., 2001, *A&A*, 367, 59
- Peacock J. A., Smith R. E., 2000, *MNRAS*, 318, 1144
- Phillipps S., Shanks T., 1987, *MNRAS*, 229, 621
- Popesso P., Böhringer H., Romaniello M., Voges W., 2005, *A&A*, 433, 415
- Popesso P., Biviano A., Böhringer H., Romaniello M., 2006, *A&A*, 445, 29
- Prada F., et al., 2003, *ApJ*, 598, 260
- Prescott M., et al., 2011, *MNRAS*, 417, 1374
- Ross A. J., Brunner R. J., 2009, *MNRAS*, 399, 878
- Sales L., Lambas D. G., 2005, *MNRAS*, 356, 1045
- Sales L. V., Navarro J. F., Lambas D. G., White S. D. M., Croton D. J., 2007, *MNRAS*, 382, 1901
- Sales L. V., Navarro J. F., Cooper A. P., White S. D. M., Frenk C. S., Helmi A., 2011, *MNRAS*, 418, 648
- Sargent M. T., et al., 2007, *ApJS*, 172, 434
- Scarlata C., et al., 2007, *ApJS*, 172, 406
- Schechter P., 1976, *ApJ*, 203, 297
- Scoville N., et al., 2007, *ApJS*, 172, 38
- Sersic J. L., 1968, *adga.book*,
- Seljak U., 2000, *MNRAS*, 318, 203
- Skibba R. A., Sheth R. K., 2009, *MNRAS*, 392, 1080
- Simard L., 1998, *ASPC*, 145, 108
- Simon J. D., Geha M., 2007, *ApJ*, 670, 313
- Simon P., Hettterscheidt M., Wolf C., Meisenheimer K., Hildebrandt H., Schneider P., Schirmer M., Erben T., 2009, *MNRAS*, 398, 807
- Smith R. M., Martínez V. J., Graham M. J., 2004, *ApJ*, 617, 1017
- Somerville R. S., Primack J. R., 1999, *MNRAS*, 310, 1087
- Somerville R. S., 2002, *ApJ*, 572, L23
- Spergel D. N., Steinhardt P. J., 2000, *PhRvL*, 84, 3760
- Springel V., White S. D. M., Tormen G., Kauffmann G., 2001, *MNRAS*, 328, 726
- Springel V., et al., 2005, *Natur*, 435, 629
- Spergel D. N., et al., 2003, *ApJS*, 148, 175
- Springel V., et al., 2005, *Natur*, 435, 629
- Tal T., Wake D. A., van Dokkum P. G., 2012, *ApJ*, 751, L5
- Tasitsiomi A., Kravtsov A. V., Wechsler R. H., Primack J. R., 2004, *ApJ*, 614, 533
- Tollerud E. J., Bullock J. S., Strigari L. E., Willman B., 2008, *ApJ*, 688, 277
- Tollerud E. J., Boylan-Kolchin M., Barton E. J., Bullock J. S., Trinh C. Q., 2011, *ApJ*, 738, 102
- Tal T., Wake D. A., van Dokkum P. G., van den Bosch F. C., Schneider D. P., Brinkmann J., Weaver B. A., 2012, *ApJ*, 746, 138
- Vader J. P., Sandage A., 1991, *ApJ*, 379, L1
- Vale A., Ostriker J. P., 2004, *MNRAS*, 353, 189
- Walsh S. M., Willman B., Jerjen H., 2009, *AJ*, 137, 450
- Wang L., Li C., Kauffmann G., De Lucia G., 2007, *MNRAS*, 377, 1419
- Wang W., White S., in preparation

- Weinmann S. M., van den Bosch F. C., Yang X., Mo H. J., 2006, MNRAS, 366, 2
- Weinmann S. M., van den Bosch F. C., Yang X., Mo H. J., Croton D. J., Moore B., 2006, MNRAS, 372, 1161
- Weinmann S. M., Lisker T., Guo Q., Meyer H. T., Janz J., 2011, MNRAS, 416, 1197
- Westra E., Geller M. J., Kurtz M. J., Fabricant D. G., Dell’Antonio I., 2010, PASP, 122, 1258
- White S. D. M., Frenk C. S., 1991, ApJ, 379, 52
- White S. D. M., Rees M. J., 1978, MNRAS, 183, 341
- Willman B., Governato F., Dalcanton J. J., Reed D., Quinn T., 2004, MNRAS, 353, 639
- Yang X., Mo H. J., van den Bosch F. C., Pasquali A., Li C., Barden M., 2007, ApJ, 671, 153
- Yang X., Mo H. J., van den Bosch F. C., 2003, MNRAS, 339, 1057
- York D. G., et al., 2000, AJ, 120, 1579
- Yoshida N., Springel V., White S. D. M., Tormen G., 2000, ApJ, 544, L87
- Zandivarez A., Martínez H. J., Merchán M. E., 2006, ApJ, 650, 137
- Zaritsky D., Smith R., Frenk C., White S. D. M., 1997, ApJ, 478, 39
- Zaritsky D., Smith R., Frenk C., White S. D. M., 1993, ApJ, 405, 464
- Zavala J., Jing Y. P., Faltenbacher A., Yepes G., Hoffman Y., Gottlöber S., Catinella B., 2009, ApJ, 700, 1779
- Zhao D. H., Jing Y. P., Mo H. J., Börner G., 2009, ApJ, 707, 354
- Zheng Z., et al., 2005, ApJ, 633, 791

APPENDIX A: DATA SYSTEMATICS AND COMPLETENESS

A1 SDSS Photometry Systematics

As mentioned by Mandelbaum et al. (2005, 2006) and also discussed in the SDSS/DR8 paper (Aihara et al. 2011), the magnitudes of faint objects close to brighter galaxies are affected by systematic problems related to sky subtraction and deblending. This results in an apparent over- or under-abundance of faint galaxies close to bright ones. This is potentially a critical problem for our study, since we evaluate the mean number of satellites surrounding some set of primaries by counting all faint neighbours in the photometric catalogue and then subtracting the number of background objects that should be projected onto these same regions “at random”. We therefore test explicitly for such affects in the DR8 photometry we will use.

We take our set of isolated primary galaxies and use the techniques described in the main body of our paper to count “red” neighbours brighter than $r = 21$ in a set of annuli of fixed angular scale. We also make similar counts using a fake photometric catalogue built by randomizing the positions of the actual photometric galaxies within the survey footprint. We then accumulate both sets of counts for each annulus and for all primaries within each of the five stellar mass bins used in figure 1, and we divide the real counts by the random counts to get a normalized profile. Error bars are estimated by bootstrapping the sample of primaries. Our definition of “red” is that the colours of the

photometric galaxy should be too red for it to be at the same redshift as its primary. We estimate a stellar mass M_* for the photometric galaxy *assuming* it to be at the redshift of the primary (see section 3). We then consider any photometric galaxy with $^{0.1}(g-r) > 0.032\log_{10}M_* + 0.73$ to be a background object. (This is based on the upper envelope of a rest-frame colour versus stellar mass scatter plot for SDSS galaxies with measured redshift.) Our normalized profile is thus expected to be unity to within its statistical errors. The actual results are shown in the left panel of figure A1 for our five primary stellar mass bins.

All the profiles go nicely to unity at angular separations of an arcminute or more, This shows that our colour cuts have indeed isolated a population of background galaxies which has no significant spatial correlation with the primaries. On the other hand, there are substantial deviations from unity at smaller scale which can have either sign and are similar for the different primary mass ranges. These most likely reflect photometric errors caused by the effect of the bright galaxy on the local sky background estimate used when measuring the apparent magnitude of its faint “red” neighbour (Mandelbaum et al. 2006). At $r = 21$ the logarithmic slope of the integral r -band number counts is 0.34 dex per magnitude, so a change in the apparent surface density of background objects by a factor of 1.5 requires an effective shift of about 0.5 mag in the apparent magnitude scale.⁷ Note that the typical angular size of the primaries (characterized by $\langle\theta_{90}\rangle$, where θ_{90} is the angular scale containing 90% of the Petrosian luminosity, and indicated by the arrows in the individual panels of figure A1) is quite similar for each of our stellar mass bins and is comparable to the separations where we see substantial systematic effects.

These problems will affect the SDSS photometry both of true satellites and of background galaxies, presumably by similar amounts. We will neglect the shifts in satellite magnitudes in the following since they are only substantial at separations below 20 arcsec, and so will affect very few objects. A more serious issue is whether the apparent excess (or deficit) of background galaxies will cause our background subtraction to fail, since this assumes the number density of background galaxies to be statistically uniform and independent of position on the sky relative to the primary. We estimate the size of the problem as follows. We construct a random sample by taking the full photometric catalogue and randomizing the positions of the galaxies within the survey footprint, keeping all their other properties fixed. We then accumulate the total count N_{tot} of random galaxies with $r < 21$ in each radial annulus for all the primaries in each mass bin. We multiply N_{tot} by the factor $N_{\text{red}}/N_{\text{red,rand}} - 1$. (This is the quantity on the y -axis in the left panel of figure A1 minus unity.) The result is our estimate N_{prob} of the number of apparent satellites brighter than $r = 21$ resulting from incorrect background subtraction. This systematic error will cause us difficulties if N_{prob} is comparable to the total number of satellites.

In the right panel of figure A1 we show the ratio of this estimated number of spurious satellites to the total number

⁷ Gravitational lensing could also change the apparent density of background objects, but simple estimates suggest the effect is too small to be relevant.

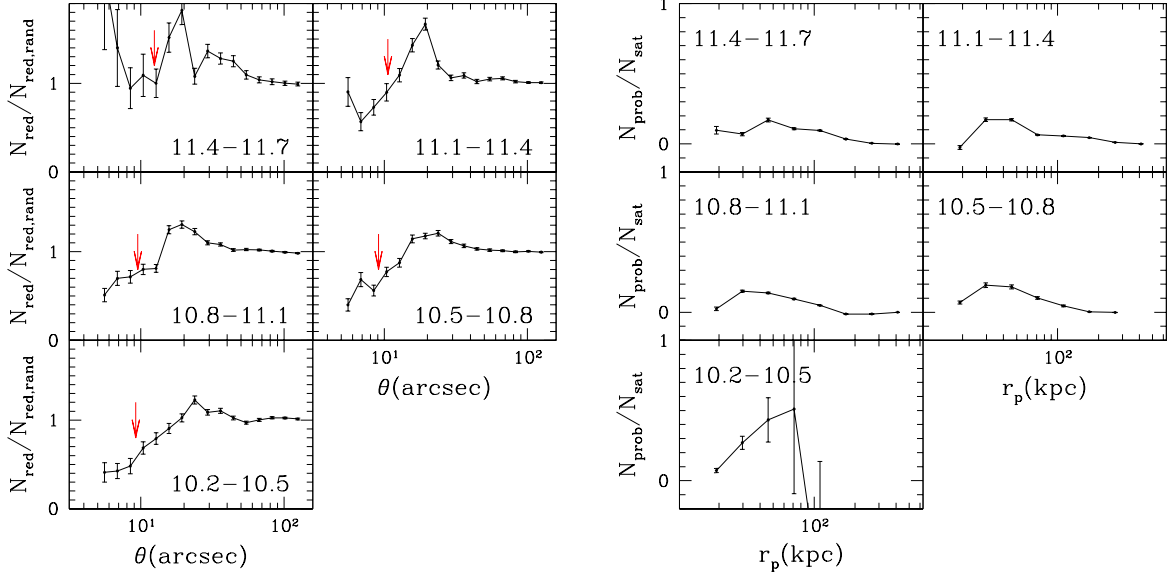


Figure A1. Left: The ratio of the number profile of “red” background galaxies with $r < 21$ around our primary sample to a similar profile for the same primaries made after randomizing the positions of the photometric galaxies within the survey footprint. The five panels refer to our five ranges of $\log M_*/M_\odot$ as indicated by the labels. The arrows show $\langle \theta_{90} \rangle$, the mean angular size of the primaries in each panel. **Right:** The ratio of our estimate of the number of “false” satellites brighter than $r = 21$ resulting from systematic errors in background subtraction to our estimate of the total number of satellites above this same apparent magnitude limit. The error bars are obtained by propagation of those in the left panel, together with bootstrapping the primary sample when estimating the satellite+background counts.

of satellites we find with $r < 21$ when the techniques discussed in section 3 are applied to the real data. It seems that this systematic error is not a problem for the four massive primary bins where $|N_{\text{prob}}|/N_{\text{sat}}$ is less than 20% on all scales. In the least massive bin, however, $|N_{\text{prob}}|/N_{\text{sat}}$ seems to be around 40% to 50% at $r_p > 30\text{kpc}$, though with pretty large error-bars. For this primary mass range the number of satellites is very small, and thus even a small misestimation of the number of background galaxies can cause a relatively big effect. Looking at the scale range corresponding to $r_p > 30\text{kpc}$ in the left panel of that bin (this is roughly $\theta > 30''$ for the relevant mean redshift $z \sim 0.06$) we find that the background density modulation required is smaller than 10%, corresponding to an apparent magnitude error of ~ 0.1 mag. A shift of this order in magnitude due to background subtraction problems does not seem implausible.

We conclude that our results are insensitive to these small-scale photometric problems except for the lowest stellar mass range we consider, where satellite counts may be significantly affected. We do not attempt to correct this systematic because we are unable to estimate sufficiently accurately how the effect depends on the photometric properties (apparent magnitude, colour, profile shape...) of the brighter and fainter images. One might hope that the effects would become smaller at brighter apparent magnitudes, but we have been unable to demonstrate this convincingly. We note that we made similar tests using DR7 photometry, finding substantially larger effects than presented here for DR8. This is our primary reason for choosing DR8 photometry when searching for satellites, even though our primary sample was defined using DR7 data.

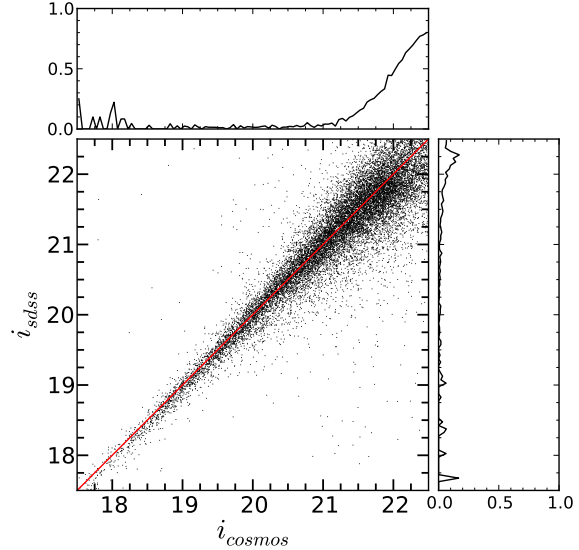


Figure A2. Scatter plot comparing SDSS and COSMOS i-band apparent magnitudes (including both galaxies and stars). Panels on the top and on the right show the fraction of COSMOS objects unmatched in SDSS and of SDSS objects unmatched in COSMOS, respectively.

A2 Completeness in SDSS

In this paper we study the properties and the distribution of satellite galaxies down to faint apparent magnitudes where identification, classification and magnitude calibration could be affected by a variety of observational factors such as see-

ing, sky brightness and extinction, in addition to the issues of photometric accuracy in the neighborhood of brighter objects which we addressed in the previous section. In this section we focus on estimating quantitatively the fraction of galaxies that might have been missed in the SDSS catalogues. We test the accuracy of star-galaxy separation in section A3, of our background galaxy subtraction methods in A4 and the influence of additional observing factors in section A5.

We investigate the completeness of the SDSS/DR8 photometric catalogue using the much deeper HST data available for the 2 squ.deg. COSMOS survey. We cross-match galaxies and stars in the COSMOS field⁸ to galaxies and stars in SDSS/DR8 and examine the failed matches in both directions. The COSMOS survey was initially conducted by HST in broad *I*-band using the Advanced Camera for Surveys (ACS) Wide-Field Channel (WFC) detector. The current COSMOS database also includes later observations from a variety of telescopes. It reaches a limiting magnitude of $I_{AB} = 28$ for point source, and $I_{AB} = 26$ for galaxies of diameter $\sim 0.5''$ (Scoville et al. 2007). This is much deeper than SDSS. The specific COSMOS catalogue used here is the Zurich Structure and Morphology catalogue⁹, which contains the measurements presented in Scarlata et al. (2007) and Sargent et al. (2007).

We further excluded COSMOS and SDSS objects which are outside the region common to both the COSMOS and the SDSS masks. The SDSS mask used here is made up of the “spherical polygons” provided on the NYU-VAGC website, and is the same as used in the main body of our paper when evaluating and correcting for edge effects. The COSMOS mask was kindly provided by Xu Kong (private communication). Objects in the Zurich COSMOS catalogue which have flag ACS_CLEAN=0, ACS_MU_CLASS=3 or JUNK_FLAG=1 are also excluded. We consider objects (galaxies or stars) to be matched in COSMOS and SDSS if their angular separation is smaller than $1.5''$.

Figure A2 is a scatter plot comparing the COSMOS and SDSS *i*-band magnitudes of matched objects. For about 4% of SDSS objects with $r < 21$ there are two matched candidates in COSMOS. This reflects the much higher resolution of the COSMOS data which allows substantially better separation of close pairs of images, double stars, merging galaxies and chance superpositions, than is possible with SDSS. In such cases, we sum the flux of all the matched COSMOS objects and compare to that of the single SDSS object.

The red straight line is a reference with $i_{cosmos} = i_{sdss}$ to guide the eye. In general, *i*-band magnitudes in COSMOS and SDSS agree with each other quite well, with a bigger scatter for fainter objects. SDSS *r*-band magnitudes of $r = 19, 20, 20.5$ and 21 correspond roughly to *i*-band magnitudes, $i = 18.6, 19.6, 20.1$ and 20.6 . For these SDSS values the scatter in COSMOS magnitudes in figure A2 is 0.277, 0.293, 0.360 and 0.367 magnitudes, respectively.

The histograms at the top and right of figure A2 show the fraction of objects in each survey which is unmatched in the other as a function of *i*-band magnitude. It is expected

that SDSS objects should be lost at the faint end, because COSMOS is much deeper. At the bright end, there are a few spikes, but the total number of objects at the bright end is small. For $i < 20.5$, we fail to match about 1% of SDSS objects in the COSMOS catalogue. This is because the COSMOS mask we are using is not identical to that used for the Zurich catalogue. In particular, it eliminates smaller regions around bright stars so we find a few SDSS objects in such regions which are not in the Zurich catalogue.

At $i \sim 20.5$, there are also about 1.5% of COSMOS objects which are unmatched in SDSS. This is only 71 objects in total, and we have looked at both SDSS and COSMOS images of these fields. We found that about 31 of these 71 objects failed to match because the angular separation between their centroid coordinates was bigger than $1.5''$. In some cases the objects are quite extended or have a close neighbour. Given the relatively poor seeing in SDSS, the determination of the coordinates of faint objects can be uncertain and so can result in failure to match to COSMOS.

On the other hand, about 40 of the 71 objects really do not have a match in SDSS. Of these, about 1/3 do indeed have an object at or close to their coordinates in the COSMOS image which SDSS failed to recognize. The remaining 2/3 do not, however, have an object at or close to their coordinates even in the COSMOS image. The Zurich Structure and Morphology catalogue also provides a cross-match with the ground based catalogue of Capak et al. (2007). Using the cross-match information provided, we found 15 out of these 40 objects do have a match in the Capak et al. (2007) catalogue, with 12 having angular separation between the two matched objects bigger than $1.5''$. The remaining objects do not have a match in the ground-based Capak et al. (2007) catalogue. We are not clear what produced these seemingly spurious objects in the COSMOS catalogue, but the fraction is indeed small ($< 1\%$).

The overall conclusion of this exercise is that incompleteness in the SDSS/DR8 photometric catalogue is at or below the 1% level at the apparent magnitude limit relevant for our analysis. This is small enough to be negligible.

A3 Star-Galaxy Separation in SDSS

SDSS carries out star-galaxy separation using the measured difference between psf (Point Spread Function) and cmodel (Composite Model) magnitudes. If $\text{psfMag} - \text{cmodelMag} > 0.145$, an object is classified as a galaxy, otherwise it is called a star. The quality of SDSS star-galaxy separation is thus unavoidably dependent on observational conditions such as seeing and sky background, and is also expected to be a function of galaxy apparent magnitude and angular size. On the other hand, COSMOS should give much more reliable star-galaxy separation because of its substantially greater depth, its much smaller point-spread function and its more uniform observing conditions. In this section we again use COSMOS data to evaluate the quality of star-galaxy separation in the SDSS.

We take galaxies in the COSMOS field and cross-match them to SDSS images, both galaxies and stars. In the match, we again used objects with $150.7 > ra > 149.5$ and $2.72 > dec > 1.65$ in order to avoid the COSMOS edge, and we again excluded objects which are obscured by the mask of either survey.

⁸ We use $150.7 > ra > 149.5$ and $2.72 > dec > 1.65$ to exclude the irregular edge of the full survey.

⁹ <http://irsa.ipac.caltech.edu/data/COSMOS/tables/morphology/>

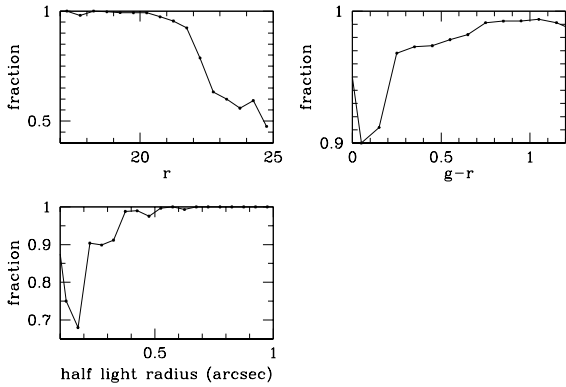


Figure A3. **Top left:** The fraction of COSMOS galaxies which have a matched SDSS galaxy (as opposed to an SDSS “star”) as a function of r -band apparent magnitude in SDSS. : **Top right:** The fraction of COSMOS galaxies which have a matched SDSS galaxy with $r < 21$, reported as a function of observed SDSS $g-r$ colour. **Bottom left:** Similar to the top right panel, but showing the matched fraction as a function of angular size as measured in COSMOS, and again limited to objects with $r < 21$ in the SDSS catalogue.

For COSMOS galaxies that have a match in SDSS (either a “galaxy” or a “star”), we show in figure A3 the fraction which are classified as galaxies by SDSS as a function of SDSS r -band apparent magnitude, SDSS $g-r$ colour and COSMOS GIM2D (Galaxy Image Two-Dimensional Simard 1998) half-light radius. The COSMOS GIM2D half-light radius is obtained by fitting a Sersic (1968) model to the galaxy image (Sargent et al. 2007).

In the top left panel of figure A3, the fraction of “correctly-classified” SDSS galaxies is close to 1 at $r < 20$ if we take COSMOS as reference, and drops significantly beyond $r = 21.5$. At $r = 21$, the fraction is about 95%. There is some discussion about star-galaxy separation on the official SDSS website¹⁰. SDSS/DR1 was compared against the COMBO-17 survey (Classifying Objects by Medium-Band Observations in 17 Filters). This much older completeness curve also drops significantly beyond $r = 21.5$, and the fraction at $r = 21$ is about 95%, in excellent agreement with our COSMOS test here.

We now consider all COSMOS galaxies with matched SDSS apparent magnitude $r < 21$, and we investigate classification success as a function of colour and angular size. The top right panel of figure A3 suggests that blue galaxies are more likely to be misclassified than red ones, although the correct fraction is always above 90%. Only about 1% of the reddest objects are misclassified. We note that the number of bluish objects ($g-r < 0.7$) is only about one-fifth of the number of red objects.

In the bottom panel of figure A3, we report galaxy classification success as a function of angular size (Sersic half-light radius from COSMOS in units of arcseconds.) The fraction starts to drop for satellite half-light radii smaller than $0.4''$, and is below 90% at $0.2''$, though never dropping below 70%. We emphasize that fewer than 100 objects in COSMOS

¹⁰ http://www.sdss3.org/dr8/imaging/other_info.php

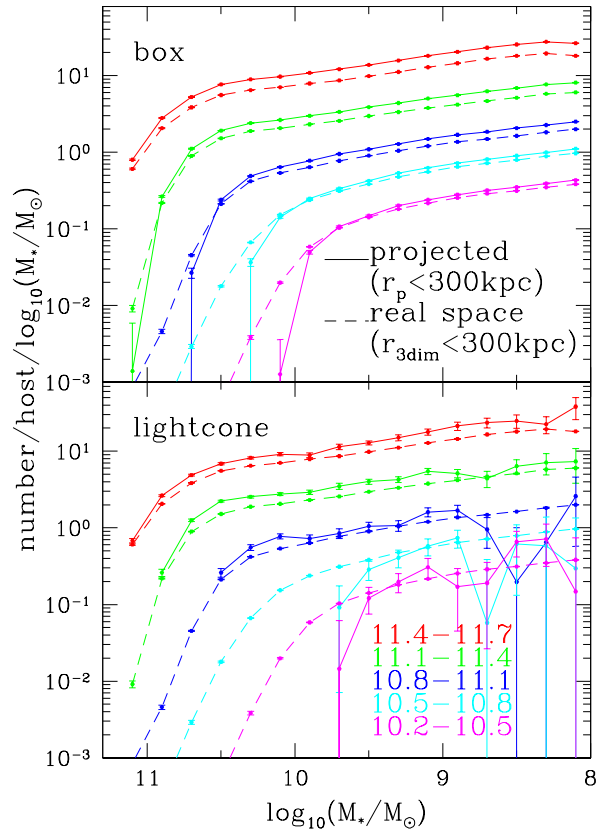


Figure A4. Tests of our background subtraction algorithms using stellar mass functions for satellites of isolated primaries in the G11 simulation separated into five ranges of primary stellar mass as indicated by colour in the legend. **Top:** Results for isolated primaries defined in a projection of the full simulation as described in the main text and shown previously in figure 6 (the solid curves) are compared with the “true” stellar mass functions defined as the mean count of satellites within 300 (or 170) kpc of these same primaries in 3D (dashed curves). **Bottom:** Results for isolated primaries defined in a full lightcone mock catalogue of SDSS/DR8 using exactly the same criteria as for the real SDSS surveys and estimated using the identical code used for the SDSS data (solid curves). The dashed curves repeat the “true” answer from the upper panel.

have $r_e < 0.2''$, which is $\sim 2\%$ of all galaxies with $r < 21$. Only about 300 have $r_e < 0.4''$.

In summary, these results together imply that not more than about 1% of galaxies brighter than $r = 21$ are misclassified as stars by SDSS, which is a remarkably small number for a 2.5m telescope working on a less than perfect site. They also imply that misclassification is a negligible problem for our purposes.

A4 Background Subtraction Tests

All our satellite abundance measurements depend critically on our ability to construct an unbiased estimate of the expected count of unrelated foreground and background galaxies projected close to each primary. This background count often exceeds the count of true satellites by a substantial factor, and the ratio of the two depends strongly on distance

from the primary and on the magnitudes of the primary and satellite galaxies. As a first test of our procedures, we randomized the positions of all galaxies in our SDSS/DR8 photometric catalogue within the SDSS footprint, while retaining all their other properties. We then repeated the analysis of luminosity and stellar mass functions which led to figures 5 and 6 keeping exactly the same sets of spectroscopic primary galaxies and using the identical code. This null test produced results which were consistent with zero within the estimated uncertainties for all satellite luminosity and stellar mass functions and around primaries in all five stellar mass ranges.

For our next tests, we used the fact that for the G11 simulation we know the true properties of the satellite distribution. We took all central galaxies in the model with stellar mass in the five mass ranges we use for our SDSS primaries and we compiled luminosity and stellar mass functions for their true satellites, defined to be companions within 300 kpc of the primary in 3-D. We then compared with the functions given in the right panels of figures 5 and 6 which were estimated in projection after correction for background contamination. The result for the stellar mass function is shown in the upper panel of Fig. A4. Although the normalizations differ slightly, as expected because of the different geometry of the regions within which satellites are counted in the two cases, the shapes of the functions agree closely in all cases, demonstrating that our “global” correction does indeed remove the background properly from our isolated galaxy sample.

Notice that this does not test aspects of our analysis concerned with converting counts from the magnitude-limited SDSS catalogues to the volume-limited statistics which we quote, for example, incompleteness corrections due to the SDSS mask, effective volume corrections, and K-corrections. We therefore took an all-sky “light-cone” mock catalogue constructed from the MS as described in Henriques et al. (2012)¹¹. We applied our SDSS mask and a magnitude limit of $r < 21$ in order to create a mock SDSS/DR8 catalogue. From this we created a mock SDSS/DR7 spectroscopic catalogue including a model for incompleteness due to fibre collisions and other observational problems. We then defined a sample of primaries using exactly the same criteria as for the real SDSS data (including a simple model of our use of photo- z 's to deal with spectroscopic incompleteness when checking for isolation) and we estimated satellite luminosity and stellar mass functions using the same code as for the real data. The results are shown in the lower panel of Fig. A4. Again agreement with the true answer is good within the now somewhat larger error bars. This agreement provides a full end-to-end test of our code.

Nevertheless, for real data, there could be additional factors which affect the accuracy of background subtraction. For example, the surface density of real galaxies on the sky could be modulated by extinction, seeing, sky brightness or proximity to other objects (see above), and thus affect our estimation of background from the whole survey which assumes background galaxies to be distributed uniformly.

Thus it is important to test the quality of our background subtraction directly on the real data.

To do so, we compare measurements of satellite mass functions for projected distances between 300kpc and 1Mpc to measurements for projected distances below 300kpc. In order to avoid complications induced by our isolation criteria which are imposed at 500 kpc and 1.0 Mpc (see Fall et al. (1976) for an example of the strong effects of such criteria), when doing this test we use all SDSS spectroscopic galaxies with $r < 16.6$ without any further selection. From our SDSS mock catalogue we estimate the mean surface densities of true satellites in these two regions to differ by factors ranging between 5.34 and 2.62 from the highest to lowest mass primaries. Since the background level should be (and is assumed to be) the same in the two regions and varies strongly with satellite mass, any error in background subtraction is expected to show up as a distortion in the shape of the satellite stellar mass function which will be much more marked in the outer region.

Figure A5 shows results for this test. Solid curves represent satellite mass functions measured within $r_p = 300$ kpc, while triangles are measurements for $1\text{Mpc} > r_p > 300$ kpc. We renormalize the $1\text{Mpc} > r_p > 300$ kpc results and replot them as dashed curves in order to compare their shape with the $r_p < 300$ kpc results. The agreement between the solid and dashed curves is quite good despite the fact that the signal-to-background ratio changes by a factor of 3.5 on average. This is both encouraging and interesting. Not only does it suggest that our background subtraction is working well, the close similarity in shape also demonstrates a significant regularity of the observed HOD, since the $r_p < 300$ kpc results are dominated by satellites in the same halo as the primary and the $1\text{Mpc} > r_p > 300$ kpc results by companions in other haloes, at least for the lower mass primaries.

It is clearly important to carry out a similar test for the sample of isolated galaxies which we analyse in this paper. For these objects, we need to examine the accuracy of background subtraction within 300 kpc, since this is the outer radius to which we count companions and lies well inside the smallest radius at which we apply an isolation criterion (500 kpc). We therefore split the region within 300 kpc into two disjoint subregions by radius. We choose the radius separating the two subregions so that they would be expected to contain equal numbers of satellites if these followed the projected NFW profile inferred for the dark matter. We list in table A1 the radial boundaries we adopt for each of our five different primary mass ranges.

The top panel of figure A6 shows satellite stellar mass functions as in figure 6 but now split to display results separately for the two subregions. Solid and dashed curves give results for the inner and outer regions, respectively. Their normalizations do not agree exactly, showing that the radial profiles are not consistent with the NFW profiles we adopted when setting the boundaries. For primaries in the two highest stellar mass ranges (the red and green curves) the amplitude in the outer annulus is higher than expected relative to that near the centre. For primaries in the two lowest stellar mass ranges (the cyan and pink curves) the opposite appears true, although the measurements are quite noisy. Thus, the inner radial distribution of satellites is shallower than NFW for massive primaries, and it could be steeper than NFW through the main body of the halo for low mass primaries.

¹¹ This catalogue is available at <http://www.mpa-garching.mpg.de/millennium>.

Table A1. Boundaries of the subregions used for testing background subtraction.

Range in primary $\log M_*/M_\odot$	11.7-11.4	11.1-11.4	10.8-11.1	10.5-10.8	10.2-10.5
Inner region	15-150 (kpc)	15-135	15-120	15-110	15-75
Outer region	150-300 (kpc)	135-300	120-300	110-300	75-170

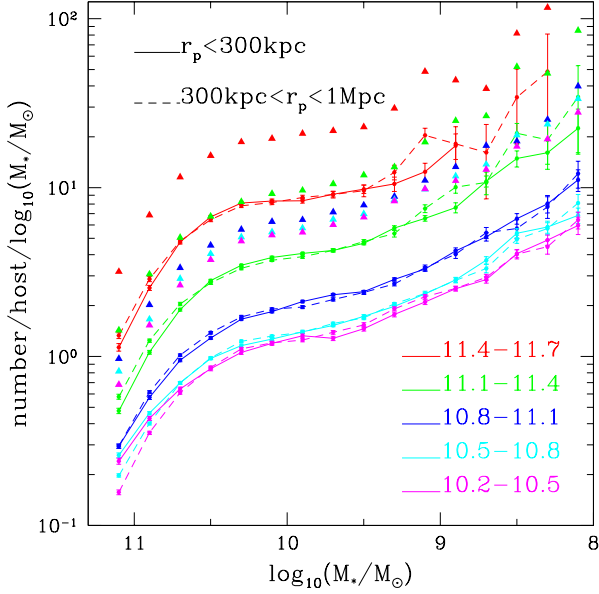


Figure A5. Stellar mass functions for companions projected within 300kpc (solid curves) and in the range $1\text{Mpc} > r_p > 300\text{kpc}$ (triangles) of primary galaxies in five disjoint stellar mass ranges. The primaries in this plot are spectroscopic galaxies with $r < 16.6$ but with no isolation criteria applied. Curves and symbols of different colour correspond to different stellar mass ranges for the primaries, as indicated by the legend. Dashed curves show the $1\text{Mpc} > r_p > 300\text{kpc}$ results renormalized in amplitude in order to compare their shape to the $< 300\text{kpc}$ results.

We will leave detailed discussion of satellite radial profiles to Wang & White which is in preparation.

Despite the difference in amplitude, the dashed and solid red, green and blue curves agree in shape quite well, except possibly at the lowest masses where statistics are relatively poor. The dashed cyan and pink curves are very noisy, but within their uncertainties they are also consistent in shape with the solid curves.

The bottom panel of figure A6 shows the ratio of the mean number of background galaxies to the mean number of satellites as a function of satellite stellar mass for each of the primary samples shown in the top panel. Solid and dashed curves again refer to the inner and outer regions. For the most massive primaries (the red curves) satellites substantially outnumber background galaxies at high mass, and are comparable in number at low mass. For the green curves, the background count already exceeds the number of satellites at almost all masses, while for the blue, cyan and pink curves, it is substantially larger, particularly for lower mass satellites and in the outer annulus. For these lower mass primaries the ratio of background to satellites

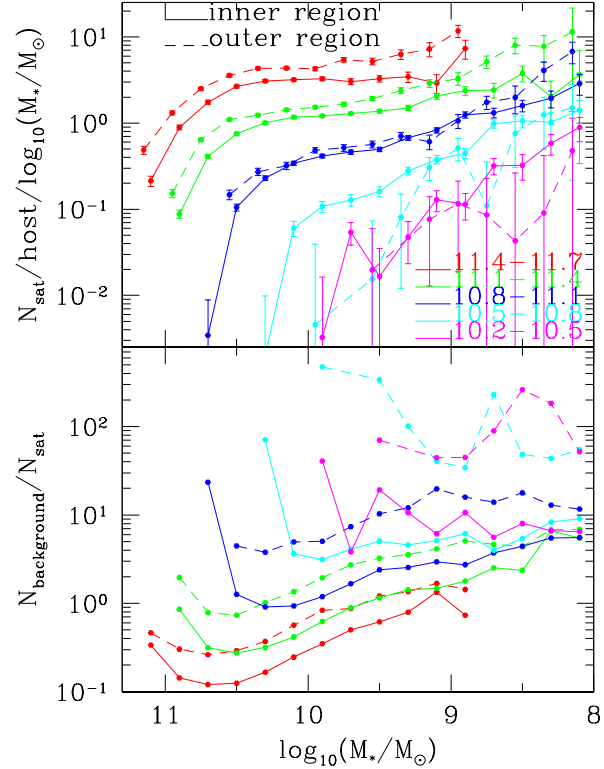


Figure A6. Top: Stellar mass functions for satellites of isolated primaries separated into five ranges of primary stellar mass as indicated by colour in the legend. The results shown before in figure 6 are split into disjoint inner (solid curves) and outer (dashed curves) regions as listed in table A1. **Bottom:** The ratio between the mean numbers of background and of satellite galaxies as a function of satellite stellar mass. Curves with different colour and line type have the same meaning as in the top panel.

in the outer annulus is almost an order of magnitude higher than in the inner region. For the blue curves, where the mass functions have high signal-to-noise over the widest satellite mass range, the background-to-satellite ratio ranges from unity to about 5.5 in the inner region and from 4 to 20 in the outer annulus. Given the large values of these corrections and their strong variation with satellite mass and radius, it is gratifying that the corresponding stellar mass functions agree in shape as well as they do.

A5 Other Observational Factors

In this section we investigate whether other observational factors such as Galactic latitude, extinction, seeing and sky brightness introduce systematic effects in our results. We start with our sample of isolated primaries with $11.1 >$

$\log M_*/M_\odot > 10.8$ and subdivide it into pairs of disjoint approximately equal subsamples based on Galactic latitude, r -band extinction, seeing, sky brightness at the time of observation of each object and redshift. In each case we estimate satellite stellar mass functions for the two subsamples separately and then compare the results.

In the top two panels of figure A7, we compare stellar mass functions for primaries with Galactic latitude $b > 60^\circ$ and with $b < 60^\circ$ as indicated by the legends. (Numbers in brackets give the mean Galactic latitudes of the two subsamples.) The two panels differ in that at top left the background was estimated globally using the survey as a whole and then applied in the same way to primaries in each subsample, while at top right the background for each subsample was estimated separately from its own half of the SDSS footprint. A clear difference at low mass is seen between the two stellar mass functions in the top left panel, but is almost entirely eliminated in the top right panel. This reflects a difference in mean surface density of about 3.5% between the two regions for galaxies with (extinction-corrected) apparent magnitude in the range $21 > r > 20$, with the low Galactic latitude region having lower mean surface density.

It is unclear what causes this problem. Clearly there are more stars and greater dust optical depths at low Galactic latitude. However, misclassification of stars as galaxies would *increase* the apparent galaxy density at low latitudes and there is no obvious reason why galaxies would be more likely to be misclassified as stars at low latitude. Moreover, unless the COSMOS field analyzed above is atypical, star-galaxy separation in the SDSS is too accurate for errors to produce such a change in mean “galaxy” density. Effects due to inappropriate correction for reddening also seem to be excluded by the explicit extinction test we discuss next.

The central and lower left panels of figure A7 show that our satellite stellar mass function results do not differ significantly for regions observed through greater extinction, in poorer seeing, or against a brighter sky. In all three cases the two halves of the sample give results which appear in good agreement. Only for the lowest mass objects where the uncertainties become substantial is there any hint of a disagreement between the red and the black curves, and even here no consistent pattern emerges. Thus none of the observational factors discussed here appears to significantly bias our results.

A6 A bias with redshift?

In the bottom right panel of figure A7, we split the primary sample according to redshift. There is a significant difference in satellite stellar mass function between two resulting subsamples, corresponding to a difference in amplitude by about a factor of 1.5 with the nearer primaries having more satellites. The mean redshifts of the two subsamples are 0.0379 and 0.0713, and we have checked in the G11 simulation that negligible evolution in satellite abundance is expected over such a small redshift interval. Further, the distributions of stellar mass and intrinsic colour are indistinguishable for the two sets of primaries, so a significant “cosmic variance” difference between the samples appears excluded. The discrepancy cannot be a consequence of our isolation criteria, since it persists for stellar mass functions like those of figure A6 which count companions around spectroscopic galax-

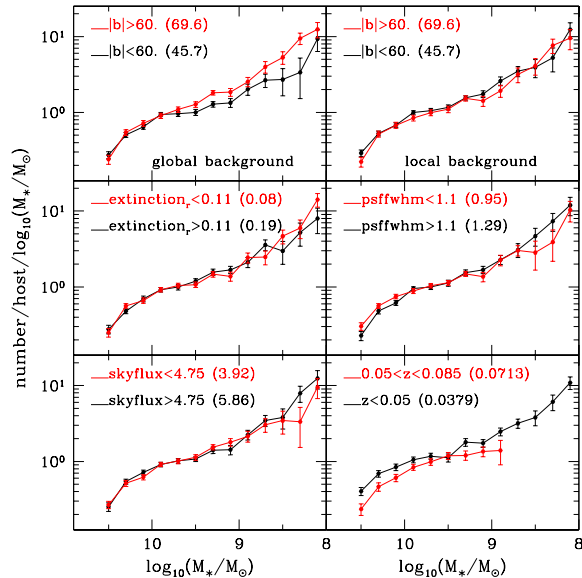


Figure A7. Stellar mass functions for isolated primaries with $11.1 > \log M_*/M_\odot > 10.8$, split into subsamples of approximately equal size based on Galactic latitude, r -band extinction, seeing, sky brightness and redshift, as indicated by the legends. The top two panels show the same subsamples split according to Galactic latitude but corrected using a global background estimate on the left and a background estimated separately for each subsample on the right. Numbers in the parentheses following the legends in each panel give mean values of the separating quantity for each of the two subsamples.

ies without imposed isolation criteria. An identical analysis of isolated galaxies from the mock SDSS survey we constructed from the MS light-cone finds no difference between the satellite stellar mass functions when split by redshift in the same way. Thus the discrepancy must reflect a property of the real data which is not included in the simulation and in construction of the mock catalogue.

In order to search for clues to the origin of this bias, we compare the distributions of rest-frame colour and size in these two redshift bins for satellites with $9.5 > \log M_*/M_\odot > 8.75$ which are projected within 300 kpc of isolated primaries with $11.1 > \log M_*/M_\odot > 10.8$. Results are presented in figure A8. From the satellite colour distributions in the left panel, it appears that the higher redshift subsample is missing predominantly red satellites. The right panel indicates, however, that these “missing” galaxies are similar in size to the remaining satellites. The colours, angular sizes and surface brightnesses of such objects are in the range where SDSS observations detect and correctly classify galaxies without difficulty. Hence there is no obvious reason why they should be missed if, in reality, they are present.

Currently, we have no explanation for this apparent dependence on redshift. We have verified that it appears in very similar form for other primary mass ranges. Given that the luminosity/stellar mass functions presented in the main body of this paper are a combination of counts around primaries at different redshifts, and that higher redshift primaries contribute to the counts of brighter/more massive satellites, this apparent decrease in satellite abundance with redshift will result in measurement of a steeper slope for the

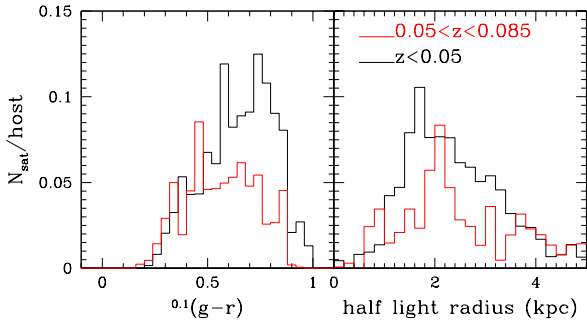


Figure A8. **Left:** Rest-frame colour distributions, normalized per primary, for satellites with $9.5 > \log M_*/M_\odot > 8.75$ projected within 300 kpc of isolated primaries with $11.1 > \log M_*/M_\odot > 10.8$ and split according to redshift at $z = 0.05$. **Right:** Size distributions, also normalized per primary, for the same two sets of satellites.

full sample as compared to either the black or the red curve in the bottom right panel of figure A7. The measured low-mass slopes for these two subsamples are -1.444 (black) and -1.390 (red). The corresponding low-mass slope for the stellar mass function in figure 6 is -1.455 (see table 1), which is indeed steeper, as expected. The difference is less than 5%, however, so this residual unidentified systematic should have only a small effect on our conclusions.